Glauber theory of final-state interactions in $A(e,e'p)$ scattering

N. N. Nikolaev

IKP(Theorie), Forschungszentrum Jülich GmbH, D-52425 Jülich, Germany
and L. D. Landau Institute for Theoretical Physics, 117940 Moscow, Russia

J. Speth

IKP(Theorie), Forschungszentrum Jülich GmbH, D-52425 Jülich, Germany

B. G. Zakharov

L. D. Landau Institute for Theoretical Physics, 117940 Moscow, Russia

We develop the Glauber-theory description of the final-state interaction (FSI) in quasielastic $A(e,e'p)$ scattering. The important new effect is an interaction between the two trajectories which enter the calculation of the FSI-distorted one-body density matrix and are connected with incoherent elastic rescatterings of the struck proton on spectator nucleons. We demonstrate that FSI distortion of the missing-momentum distribution is large over the whole range of missing momenta. The important finding is that incoherent elastic rescattering of the ejected proton leads to strong quantum-mechanical distortions of both the longitudinal and transverse missing-momentum distributions. It is shown that allowance for the finite longitudinal size of the interaction region associated with proton-nucleon collision neglected in the standard Glauber model drastically affects the theoretical predictions at high longitudinal missing momentum. We also find very large corrections to the missing-momentum distribution calculated within the local-density approximation. © *1996 American Institute of Physics.* [S1063-7761(96)00406-4]

1. INTRODUCTION

In recent years much experimental and theoretical effort has been devoted to the investigation of final-state interaction (FSI) effects in quasielastic $A(e,e'p)$ scattering at high Q^2. The strength of the FSI is usually characterized by the nuclear transparency T_A defined as the ratio of the experimentally measured cross section to the theoretical cross section calculated in the plane-wave impulse approximation (PWIA). The strong interactions that the struck proton undergoes during its propagation through the nuclear medium causes T_A to deviate from unity. It is expected,[1,2] however, that, at asymptotically high Q^2, T_A must tend to unity due to the color transparency (CT) phenomenon in QCD[3-5] (see Ref. 6 for a recent review on CT). From the point of view of multiple-scattering theory this effect corresponds to a cancellation between the rescattering amplitudes with elastic (diagonal) and inelastic (off-diagonal) intermediate states. These coupled-channel effects only become important at sufficiently high Q^2, and recent quantum-mechanical analysis[7] of $A(e,e'p)$ scattering has shown that the CT effect from the off-diagonal contribution to FSI is still weak in the region $Q^2 \lesssim 10$ GeV^2, which was confirmed by the NE18 experiment.[8] Thus, there are reasons to expect that in the region $Q^2 \sim 2$–10 GeV^2, which is particularly interesting for future high-statistics experiments at CEBAF, FSI in $A(e,e'p)$ scattering will be dominated by elastic rescattering of the struck proton on the spectator nucleons. In this region of Q^2 the typical kinetic energy of the struck proton $T_{kin} \approx Q^2/2m_p \gtrsim 1$ GeV is quite large, and FSI can be treated within the standard Glauber model.[9] The purpose of the present paper is to present a Glauber-theory description of the missing-momentum distribution in inclusive $A(e,e'p)$ scattering. We focus on the region of missing momenta $p_m \lesssim k_F$ (here $k_F \sim 250$ MeV/c is the Fermi momentum). Such an analysis is interesting for several reasons.

First, understanding the $\mathbf{p}_m$-dependence of FSI effects is necessary for a quantitative interpretation of the data from the NE18 experiment[8] and from future experiments at CEBAF. The point is that experimentally one measures the $A(e,e'p)$ cross section only in a restricted acceptance window in the missing momentum. Because FSI affects the missing-momentum distribution in comparison with the PWIA case, the absolute value and the energy dependence of the experimentally measured nuclear transparency will be different for different kinematical domains. Consequently, understanding the $\mathbf{p}_m$- and Q^2-dependence of the conventional FSI effects is imperative for disentangling the small CT effects at CEBAF and beyond.

Secondly, another CT effect which can be obscured by FSI is the forward-backward asymmetry of nuclear transparency[10-12] about $p_{m,z}=0$ (as usual we choose the z axis parallel to the three-momentum of the virtual photon). The CT induced forward-backward asymmetry increases with Q^2. However, similar forward-backward asymmetry is generated by FSI even at the level of elastic rescattering of the struck proton from the spectator nucleons. This is a consequence of the nonzero real part of the pN elastic scattering amplitude. Qualitative estimates[6] show that for $Q^2 \lesssim 10$ GeV^2 the FSI-induced asymmetry can overcome the CT-induced effect. For this reason, the interpretation of results from the future CEBAF data on the forward-backward asymmetry as a

signal for the onset of CT requires an accurate calculation of the missing-momentum distribution in the Glauber model.

Last but not least, the quantitative theory of FSI in quasi-elastic $A(e,e'p)$ scattering is interesting from the point of view of the nuclear physics as well. At high momenta, the single-particle momentum distribution (SPMD) is sensitive to short range NN correlations (SRC) in nuclei. Because of FSI effects, the experimentally measured missing-momentum distribution in inclusive $A(e,e'p)$ scattering may differ considerably from the real SPMD. There has already been extensive work on FSI effects in the optical model approach to distorted-wave impulse approximation (DWIA) (for a detailed review with many references to earlier works see Ref. 13). The novel aspect of FSI we focus on in this paper can be called the interaction of the two trajectories which enter the calculation of the FSI-modified one-body density matrix. This interaction of the two trajectories is induced by the incoherent rescatterings of the struck proton off the spectator nucleons and is missed in the standard formulation of DWIA. Several aspects of the interaction of the two trajectories via incoherent rescattering, mostly at large p_m, were discussed in recent papers.[14–17] Of special relevance to the present paper is an observation[14] that the effects of FSI due to incoherent rescattering overwhelm the SRC effects by the large parameter

$$\frac{\text{FSI (inc. resc.)}}{\text{SRC}} \approx \frac{1}{2} \left[\frac{\sigma_{\text{tot}}(pN)}{4\pi r_c^2} \right]^2 \left(\frac{R_A}{r_c} \right)^2 \gg 1. \qquad (1)$$

Still another novel quantum-mechanical effect found in Ref. 14 is a nontrivial interference of the FSI and SRC effects, which is quite strong in the $^4\text{He}(e,e'p)$ scattering, but is suppressed in heavy nuclei with respect to the incoherent rescattering effect by the small parameter $\sim r_c/R_A$. Here $\sigma_{\text{tot}}(pN)$ is the proton-nucleon total cross section, $r_c \sim 0.5$ fm is the SRC radius [numerically, in the gigaelectronvolt energy range the pN interaction radius is similar to r_c and $\sigma_{\text{tot}}(pN) \approx 4\pi r_c^2$], and R_A is the radius of a target nucleus. Even in the lightest nucleus, deuterium, in which the probability of FSI is still very small, FSI effects are quite strong.[15] Furthermore, incoherent rescattering of the struck proton from the spectator nucleons do substantially modify the longitudinal missing-momentum distribution compared with the SPMD. It leads to large tails in the missing-momentum distribution at high $|p_{m,z}|$, which are of a purely quantum-mechanical origin and defy the classical treatment. This vast variety of FSI phenomena justifies looking at the salient features of FSI effects and, in particular the effects of incoherent rescattering, in a simplified shell model neglecting SRC effects [the full analysis of $^4\text{He}(e,e'p)$ scattering is presented elsewhere.[18]] In heavier nuclei, which we study in the present paper, FSI distortions of the missing-momentum distribution turn out to be strong even in the region of relatively small momenta, $p_m \lesssim 300$ MeV/c. We find that the inclusion of incoherent rescattering causes the p_m distributions to depart substantially from predictions of the conventional DWIA over the whole range of missing momenta.

One important finding from our study of FSI is a natural applicability limit for the Glauber formalism in the case of the $A(e,e'p)$ reaction. It is connected with the finite longi-tudinal size of the interaction region for proton-nucleon collisions, which is about the proton radius. This is neglected in standard applications of multiple-scattering theory, what leads to an anomalously slow decrease $(\propto |p_{m,z}|^{-2})$ of the missing-momentum distribution at high $p_{m,z}$. The physical origin of this anomalous behavior is an incorrect treatment in the Glauber model of the incoherent rescattering of the struck proton on the adjacent spectator nucleons, when the longitudinal separation between the struck proton and spectator nucleons is comparable with the proton size. Our estimates show that uncertainties due to finite proton size effects can be large only for $|p_{m,z}| \gtrsim 500$ MeV/c. In this region of $|p_{m,z}|$, besides the short range NN correlations, the experimentally measured missing-momentum distribution becomes sensitive to the finite proton size effects in FSI, which makes the experimental study of NN correlations much more difficult. It is important that this novel sensitivity of the missing-momentum distribution at high $|p_{m,z}|$ to the proton size does not disappear at high Q^2 and persists in the coupled-channel multiple-scattering theory when the CT effects for the inelastic (off-diagonal) rescattering of the struck proton are included. One must be aware of this effect in the interpretation of the high-p_m experimental data from future experiments at large Q^2.

Our paper is organized as follows. In Sec. 2 we derive the Glauber theory formulas for calculation of the missing-momentum distribution in $A(e,e'p)$ scattering. We also discuss briefly the generalization of our formalism to the case with allowance for CT effects. We conclude Sec. 2 with comments on other works on the application of the Glauber model to $A(e,e'p)$ reaction. The subject of Sec. 3 is the detailed comparison of the Glauber model with the optical potential approach. Here we emphasize the importance of the novel FSI effect of distortion of the one-body density matrix by incoherent elastic rescattering of the struck proton in the nuclear medium, which emerges in the Glauber model naturally and is missed in the optical model. We conclude Sec. 3 with comments on the formal analogy between the optical potential treatment of the FSI and the Glauber formalism as applied to the exclusive $A(e,e'p)$ scattering. In Sec. 4 we derive the multiple-scattering series for the transverse missing-momentum distribution. We show that the $p_{m\perp}$ distribution can be formally represented in a form when all the effects of quantum-mechanical distortion for coherent elastic rescatterings are reabsorbed in the local $p_{m\perp}$ distribution, which then is convolved with the differential cross section of multiple incoherent elastic rescattering of the struck proton on the spectator nucleons. In Sec. 5 we discuss in detail how the incoherent rescattering of the struck proton on the spectator nucleons significantly affects the longitudinal missing-momentum distribution at high $|p_{m,z}|$. The qualitative quantum-mechanical analysis of this phenomenon is presented and the emerging applicability limits of the Glauber model are discussed. In Sec. 6 we present our numerical results. The summary and conclusions are presented in Sec. 7.

One remark on our terminology is in order: In the present paper we consider the $A(e,e'p)$ reaction without production of new hadrons. We will use the term "inclusive

$A(e,e'p)$ scattering'' for the process in which one sums the cross section over the undetected final state of the residual nucleus. The term "exclusive $A(e,e'p)$ scattering" will be used for process in which there is only one knocked-out nucleon (the struck proton).

2. FSI AND THE MISSING-MOMENTUM DISTRIBUTION IN THE GLAUBER THEORY

We begin with the kinematics of quasielastic $A(e,e'p)$ scattering. Following the usual practice,[13,19] we assume that the differential cross section of the $A(e,e'p)$ reaction can be expressed through the half-off-shell ep-cross section, σ_{ep}, and the distorted spectral function, $S(E_m,\mathbf{p}_m)$, as

$$\frac{d\sigma}{dQ^2d\nu dp d\Omega_p} = K\sigma_{ep}S(E_m,\mathbf{p}_m). \qquad (2)$$

Here K is the kinematic factor, ν and $\mathbf{q}$ are the (e,e') energy and momentum transfer, $Q^2=q^2-\nu^2$, the struck proton has momentum $\mathbf{p}$ and energy $E(p)=T_{kin}+m_p$, the missing momentum and energy are defined as $\mathbf{p}_m=\mathbf{q}-\mathbf{p}$ and $E_m=\nu+m_p-E(p)$ and the z-axis is chosen along $\mathbf{q}$. Equation (2) is written under the assumption that the difference between the spectral functions corresponding to absorption of the longitudinal (L) and transverse (T) photons, connected with the spin effects in FSI, can be neglected. We ignore spin effects in FSI because when the energy of the struck proton is large they become small. Since we do not distinguish between the longitudinal and transverse spectral functions, below we treat the electromagnetic current as a scalar operator. Also, note that Eq. (2) is related to the cross section averaged over the azimuthal angle between the missing momentum and the (e,e') reaction plane, which does not contain the LT and TT interference responses.[13]

In terms of the distorted spectral function the nuclear transparency in a certain acceptance domain D of the missing energy and the missing momentum can be written as

$$T_A(D) = \frac{\int_D dE_m d^3p_m S(E_m,\mathbf{p}_m)}{\int_D dE_m d^3p_m S_{\text{PWIA}}(E_m,\mathbf{p}_m)}. \qquad (3)$$

Here $S_{\text{PWIA}}(E_m,\mathbf{p}_m)$ is the theoretical spectral function of the PWIA calculated for the vanishing FSI. The missing-momentum distribution which is of our interest in the present paper is given by

$$w(\mathbf{p}_m) = \frac{1}{(2\pi)^3}\int dE_m S(E_m,\mathbf{p}_m). \qquad (4)$$

The distorted spectral function can be written as

$$S(E_m,\mathbf{p}_m) = \sum_f |M_f(\mathbf{p}_m)|^2 \delta\,(E_m+E_{A-1}(\mathbf{p}_m)+m_p-m_A), \qquad (5)$$

where $M_f(\mathbf{p}_m)$ is the reduced matrix element of the exclusive process $e+A_i\to e'+(A-1)_f+p$. Then the missing-momentum distribution reads

$$w(\mathbf{p}_m) = \frac{1}{(2\pi)^3}\sum_f |M_f(\mathbf{p}_m)|^2. \qquad (6)$$

In our analysis we confine ourselves to target nuclei with large mass number $A\gg1$. Then, neglecting the center of mass correlations, we can write $M_f(\mathbf{p}_m)$ as

$$M_f(\mathbf{p}_m) = \int d^3r_1...d^3r_A\Psi_f^*(\mathbf{r}_2,...,\mathbf{r}_A)\Psi_i(\mathbf{r}_1,...,\mathbf{r}_A)$$
$$\times S(\mathbf{r}_1,...\mathbf{r}_A)\exp(i\mathbf{p}_m\mathbf{r}_1). \qquad (7)$$

Here Ψ_i and Ψ_f are the wave functions of the target and residual nucleus, respectively. The nucleon "1" is chosen to be the struck proton. For the sake of brevity, in Eq. (7) and hereafter the spin and isospin variables are suppressed. The factor $S(\mathbf{r}_1,...,\mathbf{r}_A)$, which describes the FSI of the struck proton with spectator nucleons, is given by

$$S(\mathbf{r}_1,...,\mathbf{r}_A) = \prod_{j=2}^{A} [1-\theta(z_j-z_1)\Gamma(\mathbf{b}_1-\mathbf{b}_j)], \qquad (8)$$

where $\mathbf{b}_j$ and z_j are the transverse and longitudinal coordinates of the nucleons and $\Gamma(\mathbf{b})$ is the familiar profile function of the elastic proton-nucleon scattering. (As usual we assume that the spectator coordinates may be considered as frozen during propagation of the fast proton through the nuclear medium.) For $\Gamma(\mathbf{b})$ we use the standard high-energy parametrization

$$\Gamma(\mathbf{b}) = \frac{\sigma_{tot}(pN)(1-i\alpha_{pN})}{4\pi B_{pN}}\exp\left(-\frac{b^2}{2B_{pN}}\right). \qquad (9)$$

Here α_{pN} is the ratio of the real to imaginary part of the forward elastic pN amplitude, B_{pN} is the diffractive slope describing the t-dependence of the elastic proton-nucleon cross section:

$$\frac{d\sigma_{el}(pN)}{dt} = \frac{d\sigma_{el}(pN)}{dt}\bigg|_{t=0}\exp(-B_{pN}|t|). \qquad (10)$$

In the Glauber high-energy approximation, the struck proton propagates along the straight-path trajectory and can interact with the spectator nucleon "j" only provided that $z_j>z_1$, which is the origin of the step-function $\theta(z_j-z_1)$ in the FSI factor (8). Physically, this means that we neglect the finite longitudinal size of the region where the struck proton interacts with the spectator nucleon. The consequences of this approximation will be discussed in section 5.

The sum over all the final states of the residual nucleus in Eq. (6) can be performed making use of the closure relation

$$\sum_f \Psi_f(\mathbf{r}_2',...,\mathbf{r}_A')\Psi_f^*(\mathbf{r}_2,...,\mathbf{r}_A) = \prod_{j=2}^{A}\delta^{(3)}(\mathbf{r}_j-\mathbf{r}_j'), \qquad (11)$$

which leads to

$$w(\mathbf{p}_m) = \frac{1}{(2\pi)^3}\int d^3r_1 d^3r_1'\prod_{j=2}^{A} d^3r_j \exp[i\mathbf{p}_m(\mathbf{r}_1-\mathbf{r}_1')]$$
$$\times \Psi_i(\mathbf{r}_1,\mathbf{r}_2,...,\mathbf{r}_A)\Psi_i^*(\mathbf{r}_1',\mathbf{r}_2,...,\mathbf{r}_A)$$
$$\times S(\mathbf{r}_1,\mathbf{r}_2,...,\mathbf{r}_A)S^*(\mathbf{r}_1',\mathbf{r}_2,...,\mathbf{r}_A). \qquad (12)$$

Thus, from the standpoint of the nuclear physics, the calculation of the missing-momentum distribution $w(\mathbf{p}_m)$ reduces to an evaluation of the ground-state expectation value for a special many-body operator

$$w(\mathbf{p}_m) = \langle \Psi_i | U(\mathbf{p}_m) | \Psi_i \rangle, \tag{13}$$

where

$$\langle \mathbf{r}_1', \ldots, \mathbf{r}_A' | U(\mathbf{p}_m) | \mathbf{r}_1, \ldots, \mathbf{r}_A \rangle$$

$$= \frac{1}{(2\pi)^3} \exp[i\mathbf{p}_m(\mathbf{r}_1 - \mathbf{r}_1')] \prod_{j=2}^{A} \delta^{(3)}(\mathbf{r}_j' - \mathbf{r}_j)$$

$$\times S^*(\mathbf{r}_1', \ldots, \mathbf{r}_A') S(\mathbf{r}_1, \ldots, \mathbf{r}_A). \tag{14}$$

The essential characteristic of the operator U from Eq. (14) is that it distorts the target nucleus wave function in the variables $\mathbf{r}_2, \ldots, \mathbf{r}_A$ only when some of the $\mathbf{r}_i$ are close, within the high-energy pN interaction radius, to at least one of the two straight-line trajectories beginning from the points $\mathbf{r}_1$ and $\mathbf{r}_1'$, which arise after we take the square of the reduced nuclear matrix element (7). The crucial point of the subsequent analysis is that the FSI generates a short-range interaction between these two trajectories, which will be one of the main factors in the distortion of missing-momentum distribution as compared to the SPMD.

Note that thus far we have not used the specific form of the Glauber attenuation factor (8). The obvious generalization of Eq. (12) with allowance for the CT effects is the substitution

$$S(\mathbf{r}_1, \mathbf{r}_2, \ldots, \mathbf{r}_A) \Rightarrow \frac{\langle p | \hat{S}_{3q}(\mathbf{r}_1, \mathbf{r}_2, \ldots, \mathbf{r}_A) | E \rangle}{\langle p | E \rangle}, \tag{15}$$

where $|E\rangle$ is a three-quark wave function which describes the state of the proton (the ejectile) after absorption of the virtual photon at point $\mathbf{r}_1$, and $\hat{S}_{3q}(\mathbf{r}_1, \mathbf{r}_2, \ldots, \mathbf{r}_A)$ is an operator which describes the evolution of the three-quark wave function of the struck proton as it propagates in the nuclear medium. In terms of the electromagnetic current operator $\hat{J}_{em}$, the ejectile wave function is expressed as[11]

$$|E\rangle = \hat{J}_{em}(Q)|p\rangle = \sum_i |i\rangle\langle i|J_{em}(Q)|p\rangle = \sum_i G_{ip}(Q)|i\rangle, \tag{16}$$

where $G_{ip}(Q) = \langle i|J_{em}(Q)|p\rangle$ includes the electromagnetic form factor of the proton as well as all the transition form factors for the electroexcitation of the proton, $e + p \rightarrow e' + i$. In the case of the nonrelativistic oscillator quark model the evolution operator S_{3q} can readily be computed using the path-integral technique.[20-22] It is possible to evaluate this operator also in the coupled-channel multiple scattering theory.[7] Here we restrict ourselves to the conventional, single-channel, Glauber approximation; the CT effects will be considered elsewhere.

Equations (8), (12) form the basis of the Glauber-theory calculation of the missing-momentum distribution and nuclear transparency in $A(e,e'p)$ reaction. Evidently, even neglecting the CT effects, evaluation of $w(\mathbf{p}_m)$ is quite an involved problem. For the reasons outlined in the Introduction, in this communication we confine ourselves to an

evaluation of FSI effects in the simplified shell model, which is well known to give a good description of SPMD at moderate momenta $p_m \lesssim 250$–300 MeV/c, in which the short-range NN correlations effects are known to be marginal.[23] At larger p_m SPMD will be dominated by SRC effects,[24,25] but in the p_m distribution observed in $A(e,e'p)$ scattering FSI effects are stronger than SRC effects.[14,15,18] Furthermore, in the gigaelectronvolt energy range of interest in the present paper, $B_{pN} \sim r_c^2$ holds, and FSI and SRC contributions to the transverse missing-momentum distribution are very similar to each other with the FSI effect being numerically much larger (see the inequality (1)) (this fact is also corroborated by the small correlation effect found in Ref. 26 in the case of the integral nuclear transparency). Finally, a counterdistinction between the SRC and FSI effects is the striking angular anisotropy of FSI effects versus the isotropy of the SRC contribution to the p_m distribution.

Therefore, as far as the salient features of FSI are concerned, in particular understanding of the role of the interaction between the two trajectories in the FSI factor, it is reasonable to use a simple independent-particle nuclear shell model to calculate the missing-momentum distribution in the region $p_m \lesssim k_F$. After neglect of the SRC the A-body semidiagonal density matrix $\Psi_i(\mathbf{r}_1, \mathbf{r}_2, \ldots, \mathbf{r}_A)\Psi_i^*(\mathbf{r}_1', \mathbf{r}_2, \ldots, \mathbf{r}_A)$ still contains the Fermi correlations. To carry out the integration over the coordinates of the spectator nucleons in Eq. (12) we neglect the Fermi correlations and replace the A-body semidiagonal density matrix by the factorized form

$$\Psi_i(\mathbf{r}_1, \mathbf{r}_2, \ldots, \mathbf{r}_A)\Psi_i^*(\mathbf{r}_1', \mathbf{r}_2, \ldots, \mathbf{r}_A) \Rightarrow \rho(\mathbf{r}_1, \mathbf{r}_1')\prod_{i=2}^{A}\rho_A(\mathbf{r}_i). \tag{17}$$

Here

$$\rho(\mathbf{r}_1, \mathbf{r}_1') = \frac{1}{Z}\sum_n \phi_n^*(\mathbf{r}_1')\phi_n(\mathbf{r}_1) \tag{18}$$

is the shell-model proton one-body density matrix and ϕ_n are the shell-model wavefunctions, and $\rho_A(\mathbf{r})$ is the nucleon nuclear density normalized to unity. The errors connected with ignoring the Fermi correlations must be small, because the ratio of the Fermi correlation length $l_F \sim 3/k_F$ to the interaction length corresponding to the interaction of the struck proton with the Fermi-correlated spectator nucleons, $l_{int} \sim [4\sigma_{tot}(pN)\langle n_A\rangle]^{-1}$ (where $\langle n_A\rangle$ is the average nucleon nuclear density) is a small quantity (~ 0.25). Note that the high accuracy of the factored approximation for the many-body nuclear density in the calculation of the Glauber-model attenuation factor for hadron-nucleus scattering has been well known for a long time (for an extensive review of hadron-nucleus scattering see Ref. 27).

After we use the substitution (17) in Eq. (12), the missing-momentum distribution can be written as

$$w(\mathbf{p}_m) = \frac{1}{(2\pi)^3}\int d^3r_1 d^3r_1' \rho(\mathbf{r}_1, \mathbf{r}_1')\Phi(\mathbf{r}_1, \mathbf{r}_1')$$

$$\times \exp[i\mathbf{p}_m(\mathbf{r}_1 - \mathbf{r}_1')], \tag{19}$$

where the FSI factor $\Phi(\mathbf{r}_1, \mathbf{r}_1')$ is given by

$$\Phi(\mathbf{r}_1,\mathbf{r}_1') = \int \prod_{j=2}^{A} \rho_A(\mathbf{r}_j) d^3 r_j$$

$$\times S(\mathbf{r}_1,\mathbf{r}_2,...,\mathbf{r}_A) S^*(\mathbf{r}_1',\mathbf{r}_2,...,\mathbf{r}_A). \quad (20)$$

Equation (19) is a counterpart of the conventional formula for the SPMD. Due to the dependence of the FSI factor $\Phi(\mathbf{r}_1,\mathbf{r}_1')$ on $\mathbf{r}_1$ and $\mathbf{r}_1'$, the missing-momentum distribution normalized to unity does not coincide with the SPMD. Using the Glauber formula (8), we obtain the closed analytical expression for the FSI factor (20)

$$\Phi(\mathbf{r}_1,\mathbf{r}_1') = \left[1 - \frac{1}{A} \int d^2 b \, \Gamma(\mathbf{b}_1 - \mathbf{b}) t(\mathbf{b},z_1) \right.$$

$$- \frac{1}{A} \int d^2 b \, \Gamma^*(\mathbf{b}_1' - \mathbf{b}) t(\mathbf{b},z_1')$$

$$+ \frac{1}{A} \int d^2 b \, \Gamma^*(\mathbf{b}_1' - \mathbf{b}) \Gamma(\mathbf{b}_1$$

$$\left. - \mathbf{b}) t(\mathbf{b},\max(z_1,z_1')) \right]^{A-1}, \quad (21)$$

where we introduced the partial optical-thickness function

$$t(\mathbf{b},z) = A \int_z^\infty d\xi \rho_A(\mathbf{b},\xi). \quad (22)$$

The convolution integrals in the FSI factor can further be simplified by exploiting the fact that $t(\mathbf{b},z)$ is a smooth function of the impact parameter $\mathbf{b}$ compared to the pN profile function $\Gamma(\mathbf{b})$: to zeroth order in the small parameter B_{pN}/R_A^2 (R_A is the nucleus radius)

$$\int d^2 b \, \Gamma(\mathbf{b}_1 - \mathbf{b}) t(\mathbf{b},z) \approx \frac{\sigma_{tot}(pN)(1 - i\alpha_{pN})}{2} t(\mathbf{b}_1,z). \quad (23)$$

To the same approximation,

$$\int d^2 b \, \Gamma^*(\mathbf{b}_1' - \mathbf{b}) \Gamma(\mathbf{b}_1 - \mathbf{b}) t(\mathbf{b},z)$$

$$\approx \eta(\mathbf{b}_1 - \mathbf{b}_1') \sigma_{el}(pN) t(\tfrac{1}{2}(\mathbf{b}_1 + \mathbf{b}_1'),z), \quad (24)$$

where the strong dependence on the important variable $\mathbf{b}_1 - \mathbf{b}_1'$ is concentrated in the function $\eta(\mathbf{b})$ given by

$$\eta(\mathbf{b}) = \frac{\int d^2 \Delta \, \Gamma^*(\mathbf{b} - \Delta) \Gamma(\Delta)}{\int d^2 \Delta |\Gamma(\Delta)|^2}$$

$$= \frac{1}{\pi \sigma_{el}(pN)} \int d^2 q \, \frac{d\sigma_{el}(pN)}{dq^2} \exp(i\mathbf{q}\mathbf{b})$$

$$= \exp\left(-\frac{b^2}{4 B_{pN}} \right). \quad (25)$$

We checked that for nuclear mass number $A \gtrsim 10$ the smearing corrections to Eqs. (23) and (24) change the final results for $w(\mathbf{p}_m)$ and T_A by at most 1–3% in the range of p_m considered. Finally, making use of Eqs. (21), (23), (24) and exponentiating, which is known to be a good approximation for $A \gg 1$, we obtain

$$\Phi(\mathbf{r}_1,\mathbf{r}_1') = \exp[-\tfrac{1}{2}\sigma_{tot}(pN)(1 - i\alpha_{pN}) t(\mathbf{b}_1,z_1)$$

$$- \tfrac{1}{2}\sigma_{tot}(pN)(1 + i\alpha_{pN}) t(\mathbf{b}_1',z_1')$$

$$+ \eta(\mathbf{b}_1 - \mathbf{b}_1') \sigma_{el}(pN) t(\tfrac{1}{2}(\mathbf{b}_1 + \mathbf{b}_1'),\max(z_1,z_1'))]. \quad (26)$$

(The exponentiation (26) simplifies the discussion below, it is not required in the numerical calculations.) Below we will refer to the first two terms in the exponent in Eq. (26) as $\Gamma(\Gamma^*)$ terms, and to the last one as the $\Gamma^*\Gamma$ term. Note that, were it not for the $\Gamma^*\Gamma$ terms in the exponent, the FSI factor would have factored into two independent attenuation (and distortion) factors which only depend on $\mathbf{r}$ and $\mathbf{r}'$, respectively. The $\Gamma^*\Gamma$ term expresses the interaction between the two trajectories, which is a steep function of $|\mathbf{b}_1 - \mathbf{b}_1'|$ on the scale $\sqrt{B_{pN}}$. This interaction substantially affects the observed missing-momentum distribution and will be of major concern in this paper.

Besides the three-dimensional distribution $w(\mathbf{p}_m)$, we will consider the $p_{m,z}$-integrated $\mathbf{p}_{m\perp}$ distribution, $w_\perp(\mathbf{p}_{m\perp})$, and the $\mathbf{p}_{m\perp}$-integrated $p_{m,z}$ distribution, $w_z(p_{m,z})$. Performing the relevant longitudinal and transverse momentum integrations in (19), we obtain

$$w_z(p_{m,z}) = \frac{1}{2\pi} \int d^2 b \, dz dz' \rho(\mathbf{b},z,\mathbf{b},z') \Phi_z(\mathbf{b},z,z')$$

$$\times \exp[ip_{m,z}(z - z')], \quad (27)$$

$$w_\perp(\mathbf{p}_{m\perp}) = \frac{1}{(2\pi)^2} \int d^2 b \, d^2 b' \, dz \rho(\mathbf{b},z,\mathbf{b}',z) \Phi_\perp(\mathbf{b},\mathbf{b}',z)$$

$$\times \exp[i\mathbf{p}_{m\perp}(\mathbf{b} - \mathbf{b}')], \quad (28)$$

where

$$\Phi_z(\mathbf{b},z,z') = \exp[-\tfrac{1}{2}\sigma_{tot}(pN)(1 - i\alpha_{pN}) t(\mathbf{b},z)$$

$$- \tfrac{1}{2}\sigma_{tot}(pN)(1 + i\alpha_{pN}) t(\mathbf{b},z')$$

$$+ \sigma_{el}(pN) t(\mathbf{b},\max(z,z'))], \quad (29)$$

$$\Phi_\perp(\mathbf{b},\mathbf{b}',z) = \exp[-\tfrac{1}{2}\sigma_{tot}(pN)(1 - i\alpha_{pN}) t(\mathbf{b},z)$$

$$- \tfrac{1}{2}\sigma_{tot}(pN)(1 + i\alpha_{pN}) t(\mathbf{b}',z) + \eta(\mathbf{b}$$

$$- \mathbf{b}') \sigma_{el}(pN) t(\tfrac{1}{2}(\mathbf{b} + \mathbf{b}'),z)]. \quad (30)$$

Equations (19), (26)–(30) form the basis for our Glauber-model evaluations of the missing-momentum distribution $w(\mathbf{p}_m)$ and the transparency $T_A(\mathbf{p}_m)$ in $A(e,e'p)$ scattering. As was emphasized in Sec. 1, the three-dimensional distribution (19) is particularly important for interpreting and accurately comparing with theory the experimental data taken with the limited acceptance domain D when the nuclear transparency $T_A(D)$ is defined according to Eq. (3). The early discussion of effects of the $\Gamma^*\Gamma$ terms on T_A centered on the reshuffling of the p_m distribution by incoherent rescattering from small to large transverse missing momentum[16,17] and is only applicable for $p_m \gtrsim k_F$. In the present paper we shall present the first evaluation of T_A

(NE18) with full allowance for all the distortions predicted by the Glauber model for the kinematical conditions of the NE18 experiment.[8]

The formalism expounded above is rather simple and is based upon the same ideas as the Glauber theory of diffractive hadron-nucleus interactions.[9] We gave a very detailed derivation mainly because in the current literature there exist discussions of $A(e,e'p)$ scattering within the same Glauber model, in which the important effect of interaction between the two trajectories either is missed altogether[28,29] or is not given a full treatment.[30,31] For instance, the authors of Ref. 30 in their counterpart of our FSI factor (26) put

$$\mathbf{r}_1 = \mathbf{r}_1' = (\mathbf{r}_1 + \mathbf{r}_1')/2 \tag{31}$$

and miss the rapid dependence on the $\Delta\mathbf{r}_1 = \mathbf{r}_1 - \mathbf{r}_1'$ of the $\Gamma^*\Gamma$ term in the exponent of FSI factor. In conjunction with the local-density approximation (LDA) for the one-body density matrix[32] (we comment more on this approximation below),

$$\rho(\mathbf{r},\mathbf{r}') = \rho_A(\tfrac{1}{2}(\mathbf{r}+\mathbf{r}'))W(\mathbf{r}-\mathbf{r}') \tag{32}$$

(here $W(\mathbf{r}-\mathbf{r}')$ is the Fourier transform of the SPMD), this leads to a missing-momentum distribution which is proportional to the SPMD,[30] missing all the distortion effects which, as we shall demonstrate below, are quite strong. The same criticism is relevant to an analysis[33] of quasielastic $(p,2p)$ scattering.

The fact that neglect in Ref. 30 of the absorption-factor dependence on the variable $\Delta\mathbf{r}_1$ is not justified was pointed out by author of Ref. 31. Still, these authors included the dependence of the FSI factor only on the longitudinal component of the vector $\Delta\mathbf{r}_1$, incorrectly putting in the FSI factor

$$\mathbf{b}_1 = \mathbf{b}_1' = (\mathbf{b}_1 + \mathbf{b}_1')/2 \tag{33}$$

and so missed an interaction between the two trajectories which is a steep function of $\Delta\mathbf{b}_1 = \mathbf{b}_1 - \mathbf{b}_1'$. For this reason, the approximation (33) precludes an accurate treatment of the transverse missing-momentum distribution and can not be justified. Reference 31 also used the LDA for the one-body density matrix. It is easy to show using Eqs. (19) and (26) that the approximation (33) leads to a $p_{m,x}$-integrated transverse missing-momentum distribution which is proportional to the p_z-integrated transverse SPMD. Furthermore, in the region $p_m \lesssim k_F$, where $n_f(p_m)$ may be approximated by a Gaussian, in the resulting three-dimensional missing-momentum distribution the dependence on the transverse and longitudinal components will factorize, with the $p_{m\perp}$-dependence being the same as that of the SPMD. Such a factorization cannot be correct, because the term $\propto\Gamma^*\Gamma$ in Eq. (26), which has the steepest dependence on $\Delta\mathbf{b}_1$, and the terms $\propto\Gamma(\Gamma^*)$, which are smooth function of $\Delta\mathbf{b}_1$, have quite different dependence on $z_1 - z_1'$. Our numerical results show that the three-dimensional missing-momentum distribution (19) actually has a manifestly nonfactorizable form.

To conclude the discussion of approaches of Refs. 30 and 31, one remark is in order on the LDA (32) for the one-body density matrix used in Refs. 30 and 31. The LDA is widely believed to be a very good approximation for heavy nuclei. Our numerical results show that the LDA re-

sults for the missing-momentum distribution in $A(e,e'p)$ are too crude an approximation even for nucleus mass number $A=40$. The comparison of the LDA results with those for the full-shell model density matrix (18) will be presented in Sec. 6.

3. CONNECTION BETWEEN THE GLAUBER MODEL AND THE OPTICAL-POTENTIAL APPROACH

A comparison between the Glauber formalism set up in Sec. 2 and the optical potential approach, also known as the conventional DWIA, that is usually used to describe the FSI effects in $A(e,e'p)$ scattering at low Q^2 is in order. In the DWIA the FSI effects are taken into account by introducing an optical potential $V_{opt}(\mathbf{r})$ (for a recent review with extensive references to early works see Ref. 13). Then the outgoing proton plane wave becomes distorted as a consequence of the eikonal phase factor

$$S_{opt}(\mathbf{r}) = \exp\left[-\frac{i}{v} \int_z^\infty d\xi V_{opt}(\mathbf{b},\xi) \right] \tag{34}$$

(v is the velocity of the struck proton). The missing-momentum distribution in this approach is given by Eq. (19) with the following FSI factorization

$$\Phi_{opt}(\mathbf{r}_1,\mathbf{r}_1') = S_{opt}(\mathbf{r}_1)S_{opt}^*(\mathbf{r}_1'). \tag{35}$$

The important feature of the DWIA is that the optical potential does not depend on the individual coordinates of the spectator nucleons. Thus the optical potential in the DWIA embodies an effective description of how the nuclear medium influences the wave function of the struck proton.

As a matter of fact, the Glauber attenuation factor (8) is merely a consequence of solving the wave equation for the wave function of the struck proton in the eikonal approximation. Nevertheless there is an important conceptual difference between the DWIA and the Glauber-model approach. In the DWIA the FSI effects are taken into account at the level of the wave function of the ejected proton. However, it is clear that a rigorous evaluation of the probability distribution of a subsystem (the struck proton in the case under consideration) of a process including a complex system (the system of the struck proton and spectator nucleons in our case) requires calculations at the level of the subsystem density matrix. Equations (8) and (12) embody precisely this procedure in the case of quasielastic $A(e,e'p)$ scattering. Indeed, as was mentioned above the Glauber attenuation factor (8) solves the wave equation for the outgoing proton wave function for a certain configuration of the spectator nucleons, $\tau=\{\mathbf{r}_2,...,\mathbf{r}_A\}$. (As usual, when the energy of the struck proton is high, one can neglect the motion of the spectator nucleons during the propagation of the fast struck proton through the residual nucleus.) The reduced nuclear matrix element squared which was obtained through the wave equation for the struck proton at fixed τ is averaged over the spectator nucleon positions in Eq. (12). It is clear that the averaging over τ is merely a way of evaluating the diagonal matrix element of the subsystem (the struck proton) in momentum space. In another words the difference between the treatment of the FSI effects in the DWIA approach and in the Glauber

model can be formulated as a difference in the order of operation. Schematically, the order of operations in the DWIA is as follows:

1. Averaging over the spectator nucleon positions (evaluation of the optical potential).

2. Solving the wave equation for the struck proton wave function using the effective optical potential and calculation of the reduced nuclear matrix element squared.

In the case of the Glauber model the reverse order is used:

1. Solving of the wave equation for the struck proton wave function at fixed positions of the spectator nucleons and computing of the reduced nuclear matrix element squared.

2. Averaging over the spectator nucleon positions.

In contrast to the optical potential FSI factor (35), the Glauber-model factor (26) has a nonfactorizable form due to the presence of the term $\propto \Gamma^*\Gamma$. The interaction between the two trajectories of the struck proton in the Glauber FSI factor (26) connected with $\Gamma^*\Gamma$ term is a consequence of averaging over the spectator nucleon positions after computing the matrix element squared for fixed the spectator configuration τ. The physical origin of the $\Gamma^*\Gamma$ term in the FSI factor Φ (26) is the incoherent elastic (see Sec. 4) rescattering of the struck proton on the spectator nucleons as it propagates through the target nucleus. It is precisely the sum over the nucleus excitations created by the elastic rescattering of the ejected proton which leads to the nonfactorizable expression (26).

There is a formal analogy between the optical model FSI factor (35) and the Glauber-model factor, if the $\Gamma^*\Gamma$ term in the exponential of (26) is excluded. Indeed, such a reduced Glauber attenuation factor $\Phi_{opt}^{Gl}(\mathbf{r}_1,\mathbf{r}_1')$ takes on a factored form as a function of $\mathbf{r}_1$ and $\mathbf{r}_1'$.

$$\Phi_{opt}^{Gl}(\mathbf{r}_1,\mathbf{r}_1') = S_{opt}^{Gl}(\mathbf{r}_1)S_{opt}^{Gl*}(\mathbf{r}_1'), \qquad (36)$$

with

$$\Phi_{opt}^{Gl}(\mathbf{r}) = \exp[-\tfrac{1}{2}\sigma_{tot}(pN)(1-i\alpha_{pN})t(\mathbf{b},z)]. \qquad (37)$$

The integral nuclear transparency and the missing-momentum distribution calculated with the FSI factors (26) and (36) differ substantially. Our numerical results give clearcut evidence that the $\Gamma^*\Gamma$ term in (26) becomes very important in the region $p_m \gtrsim 200$ MeV/c. This is a consequence of the short-range (in the variable $\mathbf{r}_1 - \mathbf{r}_1'$) "interaction" between the two trajectories in the FSI factor (26). It is clear that such a short-range interaction cannot be modeled in the optical-potential approach even by means of any modifications of the factored attenuation factor (35). Thus, the optical model DWIA which was successful in the region of low Q^2, cannot be extended to describe the inclusive $A(e,e'p)$ reaction at high Q^2. The essential feature of the high-Q^2 region is that in this case both the coherent rescattering of the struck proton on the spectator nucleons and the incoherent rescattering leave the direction of the proton momentum practically unchanged. For this reason they need to be treated on the same footing. In contrast, at low Q^2, when the energy of the struck proton is small, every incoherent

rescattering of the struck proton causes a considerable loss of the struck proton's energy-momentum. As a result, the flux of the outgoing proton plane wave is suppressed. This effect is modeled in the DWIA by the imaginary part of the effective optical potential. Thus, the DWIA and the Glauber model appear to be applicable to the description of $A(e,e'p)$ scattering in different kinematical domains, at low Q^2 and at high Q^2, respectively.

It is interesting that at high Q^2 the optical potential form of the Glauber-model FSI factor (36) still has a certain domain of applicability. One can show that in the shell model without NN correlations the FSI factor (36) corresponds to the situation in which the sum over the residual nucleus states includes only one-hole excitations of the target nucleus. In the multiple elastic rescattering expansion of Sec. 4 the FSI factor (36) emerges in zeroth order in the $\Gamma^*\Gamma$ term. To a certain extent, it can be identified with single-nucleon knockout exclusive $A(e,e'p)$ scattering. Indeed, in this case the index f in Eq. (7) labels the shell state of the target nucleus occupied by the struck proton. Then, neglecting the Fermi correlations between the spectator nucleons, one can write down the reduced matrix element corresponding to the removal of the proton in the state f from the target nucleus in the form

$$M_f(\mathbf{p}_m) = \frac{1}{\sqrt{Z}} \int d^3r_1 \, \exp(i\mathbf{p}_m\mathbf{r}_1)\phi_f(\mathbf{r}_1)S_{opt}^{Gl}(\mathbf{r}_1). \qquad (38)$$

Summing the squares of the matrix elements (38) over the states f immediately leads to the formula (19) with the reduced FSI factor (36) instead of the full one (26). It is worth noting that from the quantum-mechanical point of view, the FSI factor (36) describes the FSI effects from coherent rescattering of the struck proton.

Making use of the FSI factors (26) and (36), one obtains for the integral nuclear transparency in quasielastic $A(e,e'p)$ scattering

$$T_A^{inc} = \int d^2b\,dz\rho_A(\mathbf{b},z)\exp[-\sigma_{in}(pN)t(\mathbf{b},z)], \qquad (39)$$

$(\sigma_{in}(pN)=\sigma_{tot}(pN)-\sigma_{el}(pN))$ for the inclusive reaction, and

$$T_A^{exc} = \int d^2b\,dz\rho_A(\mathbf{b},z)\exp[-\sigma_{tot}(pN)t(\mathbf{b},z)], \qquad (40)$$

for the exclusive process.

Thus the integral nuclear transparency is controlled by the inelastic proton-nucleon cross section in the inclusive case and by the total proton-nucleon cross section in the exclusive one. The physical origin of this difference is obvious. The incoherent elastic rescattering of the struck proton in the nuclear medium do not reduce the flux of the ejected proton. For this reason the attenuation is controlled by the inelastic proton-nucleon cross section in the inclusive case. In the exclusive $A(e,e'p)$ reaction the struck proton is forbidden to knock out spectator nucleons through incoherent elastic rescattering. The corresponding attenuation is controlled by the total proton-nucleon cross section and $T_A^{exc} < T_A^{inc}$.

As we already emphasized, the above correspondence between the FSI factor (36) and exclusive $A(e,e'p)$ scattering takes place only in the idealized shell model. This correspondence is partly lost if short-range NN correlations are included. Indeed, $A(e,e'p)$ scattering on the proton of the correlated NN pair causes ejection of the spectator nucleon of the correlated NN pair,[24,25] and the corresponding final state will not fall into the exclusive category. However, at small missing momenta $\mathbf{p}_m$ the probability for ejection of spectators must be small, because the typical momenta of nucleons in the correlated pair are of the same order in magnitude and $\gtrsim k_F$, and triggering on small $\mathbf{p}_m$ one effectively suppresses the contribution from correlated NN pairs.

4. INCOHERENT RESCATTERING AND THE TRANSVERSE MISSING-MOMENTUM DISTRIBUTION

Equations (39) and (40) suggest that in the case of the integral nuclear transparency FSI effects admit partly a simple quasiclassical interpretation. On the other hand, it is clear that the missing-momentum distribution (19) or $T_A(\mathbf{p}_m)$ as a function of $\mathbf{p}_m$ does not admit a classical treatment. The integration over $\mathbf{r}_1$ and $\mathbf{r}_1'$ in Eq. (19) shows that the experimentally observed cross section of $A(e,e'p)$ scattering at a particular $\mathbf{p}_m$ is a result of manifestly quantum interference of amplitudes with different positions where a virtual photon strikes the proton. We would like to emphasize that in the case of the three-dimensional missing-momentum distribution (19) the FSI effects from the incoherent rescatterrings (connected with the term $\propto \Gamma^*\Gamma$ in the FSI factor (26)) taken separately also cannot be treated classically. Indeed, the lower limit in the z-integration for the term $\propto \Gamma^*\Gamma$ in Eq. (26) is equal to the maximum value of the lower limits of the z-integration in the term $\propto \Gamma$ and $\propto \Gamma^*$. This implies that on part of the struck proton's trajectory incoherent rescattering is forbidden. Hence no probabilistic interpretation of the effects connected with the $\Gamma^*\Gamma$ term in the FSI factor (26) in the case of the nonintegrated distribution (19) is possible.

An exceptional case is the $p_{m,z}$-integrated $\mathbf{p}_{m\perp}$ distribution (28), when in the FSI factor (30) the lower limits of the z-integration in the terms $\propto \Gamma(\Gamma^*)$ and $\propto \Gamma^*\Gamma$ become equal. In this unique case, the probabilistic treatment that is possible for the integral nuclear transparency (39) can to a certain extent be extended to the transverse missing-momentum distribution (28). To demonstrate this fact it is convenient to rewrite (28) in the form

$$w_\perp(\mathbf{p}_{m\perp}) = \frac{1}{(2\pi)^2} \int d^2b \; dz d^2\Delta \; \exp(i\mathbf{p}_{m\perp}\Delta)\rho$$

$$\times(\mathbf{b}+\tfrac{1}{2}\Delta,z,\mathbf{b}-\tfrac{1}{2}\Delta,z)S_{\text{opt}}^{Gl}(\mathbf{b}+\tfrac{1}{2}\Delta,z)$$

$$\times S_{\text{opt}}^{Gl*}(\mathbf{b}-\tfrac{1}{2}\Delta,z)\exp[\,\eta(\Delta)]$$

$$\times \sigma_{el}(pN)t(\mathbf{b},z)].\qquad(41)$$

Let us introduce a local transverse momentum distribution which includes all the distortions from coherent elastic scattering effects at the level of the optical form of the Glauber FSI factor (36),

$$w_{\perp,\text{opt}}(\mathbf{b},z,\mathbf{p}_{m\perp}) = \frac{1}{(2\pi)^2} \int d^2\Delta \; \exp(i\mathbf{p}_{m\perp}\Delta)\rho$$

$$\times\left(\mathbf{b}+\frac{1}{2}\Delta,z,\mathbf{b}-\frac{1}{2}\Delta,z\right)\rho_A^{-1}(\mathbf{b},z)S_{\text{opt}}^{Gl}$$

$$\times\left(\mathbf{b}+\frac{1}{2}\Delta,z\right)S_{\text{opt}}^{Gl*}\left(\mathbf{b}-\frac{1}{2}\Delta,z\right).\qquad(42)$$

This local distribution (42) is normalized as

$$\int d^2p_{m\perp}w_{\perp,\text{opt}}(\mathbf{b},z,\mathbf{p}_{m\perp}) = |S_{\text{opt}}^{Gl}(\mathbf{b},z)|^2.$$

Then, after expanding the last exponential factor in Eq. (41) in a power series, we can represent the $p_{m,z}$-integrated transverse momentum distribution in the form of the multiple incoherent elastic rescattering series

$$w_\perp(\mathbf{p}_{m\perp}) = \sum_{\nu=0}^{\infty} w_\perp^{(\nu)}(\mathbf{p}_{m\perp}),\qquad(43)$$

where the zeroth order term is given by

$$w_\perp^{(0)}(\mathbf{p}_{m\perp}) = \int d^2b \; dz\rho_A(\mathbf{b},z)w_{\perp,\text{opt}}(\mathbf{b},z,\mathbf{p}_{m\perp}),\qquad(44)$$

and the contribution of the ν-fold component for $\nu\geq 1$ is

$$w_\perp^{(\nu)}(\mathbf{p}_{m\perp}) = \frac{1}{\nu!} \int d^2b \; dz\rho_A(\mathbf{b},z)t^\nu(\mathbf{b},z)\int \prod_{i=1}^\nu d^2q_i$$

$$\times\left(\frac{1}{\pi}\frac{d\sigma_{el}(pN)}{dq_i^2}\right)w_{\perp,\text{opt}}\left(\mathbf{b},z,\mathbf{p}_{m\perp}-\sum_{j=1}^\nu \mathbf{q}_j\right).$$

$$(45)$$

Equations (43)–(45) represent $w_\perp(\mathbf{p}_{m\perp})$ in a form when all the quantum distortion effects are contained in a local missing-momentum distribution $w_{\perp,\text{opt}}(\mathbf{b},z,\mathbf{p}_{m\perp})$ computed with the FSI factor without the $\Gamma^*\Gamma$ term. The contributions (45) to the expansion (43) from the incoherent rescattering connected with the $\Gamma^*\Gamma$ term admit a probabilistic reinterpretation.

The transverse missing-momentum distribution (28) obtained using the closure relation (11) is appropriate to inclusive $A(e,e'p)$ scattering. Nevertheless, the representation (43) can be used to estimate the contribution to the cross section of this process from events with a fixed number of the knocked-out (recoil) nucleons. Our numerical results show that the dominant contribution to the transverse missing-momentum distribution in the region $p_\perp \lesssim k_F$ comes from the terms with $\nu\leq 1$. This means that the inclusive cross section of $A(e,e'p)$ scattering in the above kinematical domain is saturated by the events without ($\nu=0$) and with one ($\nu=1$) knocked-out recoil nucleon (besides the high-energy ejected proton). At higher $p_{m\perp}$ the contribution from the terms with $\nu>1$ also becomes important. From the convolution (45) it is obvious that the large-ν terms decrease more strongly with $p_{m\perp}$ and the large-$p_{m\perp}$ behavior of $w_\perp^{\nu\geq 1}(\mathbf{p}_{m\perp})$ is only sensitive to the small-$p_{m\perp}$ behavior of the SPMD. The relative contribution of the $\nu\geq 1$ terms increases with the nuclear mass number.[16] The role of incoherent rescattering in

the region $p_\perp \gtrsim k_F$ was recently discussed in Ref. 16. It was shown there, in particular, that incoherent rescattering leads to a large tail in the missing-energy distribution. In the integrand of (41) the steepest dependence on the variable Δ is contained in the last exponential factor. As a result, at high $p_\perp$ incoherent rescattering effects become more important than distortion effects and the local transverse momentum distribution (43) can be approximated by the attenuated (but undistorted) single-particle transverse momentum distribution. This approximation has been used in Ref. 16. We will see that in the region $p_\perp \lesssim k_F$ of interest in the present paper, the FSI effects connected with distortion and with incoherent rescattering are of the same order of magnitude, and both of them must be taken into account simultaneously.

One must be careful with the physical interpretation of incoherent rescattering in the $A(e,e'p)$ reaction because the expansion (43) is somewhat formal and does not imply that incoherent rescattering allow a classical treatment. For instance, as we will see below, the representation (43) even does not imply that the momentum transfers in the incoherent rescattering of the struck proton on spectator nucleons are purely transverse. For this reason, in particular, the FSI effects associated with incoherent rescattering of the struck proton in the nuclear medium cannot be modeled via the Monte-Carlo approach.

5. LONGITUDINAL MISSING-MOMENTUM DISTRIBUTION AND APPLICABILITY LIMITS OF THE GLAUBER MODEL

The failure of the quasiclassical probabilistic treatment of incoherent rescattering becomes especially evident in the case of the longitudinal missing-momentum distribution. Naively, from the classical point of view, one expects that this distribution not to be affected by the elastic rescattering of the struck proton on the spectator nucleons. In fact, as one can see from Eqs. (19), (26), because of the last term in the exponential in Eq. (26), the incoherent rescattering must affect, and have a nontrivial impact on, the longitudinal missing-momentum distribution.

It is worth noting that even from a simple qualitative quantum-mechanical consideration one can understand that the incoherent rescattering must influence the longitudinal missing-momentum distribution. If Δl is the distance between the point where the virtual photon strikes the ejected proton and the point where incoherent scattering of the spectator nucleon takes place, then the momentum transfer in the pN scattering has the uncertainty $\Delta k \sim 1/\Delta l$. For sufficiently small Δl the longitudinal momentum transfer can be comparable to the transverse one. Thus, one can see that in the region of high $|p_{m,z}|$, $p_{m\perp}$ ($|p_{m,z}| \sim p_{m\perp}$) the incoherent rescattering of the struck proton on the adjacent spectator nucleons must considerably affect the missing-momentum distribution compared to the PWIA case. Specifically, as we will see below, the $\Gamma^*\Gamma$ term in the FSI factors (26), (29) gives rise to a substantial tail at high $|p_{m,z}|$, which is missed if the optical potential form (36) of the FSI factor is used.

From the technical point of view, this sensitivity of the longitudinal missing-momentum distribution to incoherent rescattering derives from the above mentioned aspect in the

z-integration for the term $\propto \Gamma^*\Gamma$ in Eq. (26). Whereas the factor $\Phi_{\mathrm{opt}}^{Gl}(\mathbf{r}_1,\mathbf{r}_1')$ defined by Eq. (36) has a smooth behavior in the variable $\xi = z_1 - z_1'$ at the point $\xi=0$, the FSI factor (26) as a function of ξ has a discontinuous derivative with respect to ξ at the point $\xi=0$, which has its origin in the nonanalytical function $\max(z_1,z_1')$ as the lower limit of the z-integration. After the Fourier transform, the singular behavior of the integrand in Eq. (19) (and Eq. (27) as well) in the variable ξ shows up as anomalous behavior of the missing momentum distribution at high longitudinal momenta.

Let us proceed with an analysis of the longitudinal momentum distribution for the case of the $\mathbf{p}_{m\perp}$-integrated distribution (27). The absence of the integration over $\mathbf{b}-\mathbf{b}'$ makes a qualitative analysis of this case considerably simpler than for the nonintegrated one (19). It is convenient to rewrite the longitudinal FSI factor (29) in the form

$$\Phi_z(\mathbf{b},z,z') = \Phi_{z,\mathrm{opt}}^{\mathrm{in}}(\mathbf{b},z,z') C_1(\mathbf{b},z,z') C_2(\mathbf{b},z,z') \quad (46)$$

with

$$\Phi_{z,\mathrm{opt}}^{\mathrm{in}}(\mathbf{b},z,z') = \exp[-\tfrac{1}{2}\sigma_{\mathrm{in}}(pN)t(\mathbf{b},z)$$
$$-\tfrac{1}{2}\sigma_{\mathrm{in}}(pN)t(\mathbf{b},z')], \quad (47)$$

$$C_1(\mathbf{b},z,z') = \exp\left[\frac{i}{2}\,\sigma_{\mathrm{tot}}(pN)\alpha_{pN}(t(\mathbf{b},z)-t(\mathbf{b},z'))\right], \quad (48)$$

$$C_2(\mathbf{b},z,z') = \exp[-\tfrac{1}{2}\sigma_{el}(pN)|t(\mathbf{b},z)-t(\mathbf{b},z')|]. \quad (49)$$

In Eq. (46) we separated the function $\Phi_{z,\mathrm{opt}}^{\mathrm{in}}(\mathbf{b},z,z')$ from the FSI factor (29), which to a certain extent can be interpreted as the optical potential FSI factor which describes only those distortion of the plane wave connected with real inelastic interactions (absorption) of the struck proton in the nuclear medium. We will refer to the corresponding longitudinal missing-momentum distribution as $w_{z,\mathrm{opt}}^{\mathrm{in}}(p_{m,z})$. Since $\Phi_{z,\mathrm{opt}}^{\mathrm{in}}(\mathbf{b},z,z')$ is a symmetric function of z and z', the function $w_{z,\mathrm{opt}}^{\mathrm{in}}(p_{m,z})$ is even in $p_{m,z}$.

For the purposes of the qualitative analysis, one can approximate the functions $C_{1,2}(\mathbf{b},z,z')$ for $A \gg 1$ by the following expressions:

$$C_1(\mathbf{b},z,z') = \exp[-ik_1(z-z')], \quad (50)$$

$$C_2(\mathbf{b},z,z') = \exp[-k_2|z-z'|], \quad (51)$$

where

$$k_1 = \tfrac{1}{2}\sigma_{\mathrm{tot}}(pN)\alpha_{pN}\langle n_A\rangle, \quad (52)$$

$$k_2 = \tfrac{1}{2}\sigma_{el}(pN)\langle n_A\rangle, \quad (53)$$

and $\langle n_A\rangle$ is the average nuclear density.

Then, using these approximations, the longitudinal missing-momentum distribution can be cast as a convolution

$$w_z(p_{m,z}) \approx \frac{1}{2\pi}\int dk\, w_{z,\mathrm{opt}}^{\mathrm{in}}(p_{m,z}-k_1-k)c_2(k). \quad (54)$$

Here $c_2(k)$ stands for the Fourier transform of the factor C_2. Equation (54) shows clearly that the major effect of the nonzero real part of the pN-amplitude contained in the factor C_1 is a shift of the longitudinal missing-momentum distribution

by k_1.[17] In the region of $Q^2 \sim 2{-}10$ GeV^2 this shift due to the nonzero α_{pN} is quite large, $k_1 \sim 20$ MeV/c, and causes the $p_{m,z}$ distribution to be quite asymmetric about $p_{m,z}=0$.

The role of the factor C_2 is much more interesting. In the approximation (51), the Fourier transform of the factor C_2 is given by

$$c_2(k) = \int d\xi \, \exp(ik\xi)\exp(-k_2|\xi|) = \frac{2k_2}{k^2+k_2^2}. \qquad (55)$$

In the domain of Q^2 we are interested in, numerically $k_2 \sim 10{-}20$ MeV/c. Hence a strong inequality $k_2 \ll k_F$ is satisfied and $c_2(k)$ has the form of a sharp peak, much narrower than the conventional SPMD. Consequently, at $|p_{m,z}| \ll k_F$ the factor $c_2(k)$ in the convolution representation (54) acts like a δ-function and at small $|p_{m,z}|$ we have

$$w_z(p_{m,z}) \approx w_{z,\text{opt}}^{\text{in}}(p_{m,z}-k_1), \qquad (56)$$

whereas at sufficiently large $|p_{m,z}| \gtrsim k_F$ the $p_{m,z}$-dependence of $w_z(p_{m,z})$ will be controlled rather by the asymptotic behavior of $c_2(k)$, with the result that

$$w_z(p_{m,z}) \propto p_{m,z}^{-2}. \qquad (57)$$

For real finite-size nuclei, when $c_2(k)$ is evaluated from the exact expression (49), the width of the peak in the Fourier transform $c_2(k)$ will rather be controlled by the the inverse nucleus size because $k_2 \lesssim 1/R_A$. Still, due to the strong inequality $k_F \gg 1/R_A$, the resulting peak in $c_2(k)$ again turns out to be much narrower than the SPMD. Consequently, the finite nucleus size will not change the asymptotic law $c_2(k) \propto k^{-2}$, which derives only from the nonanalytical behavior of the functions (49), (51) at the point $z=z'$.

Our numerical results show that even in the region $|p_{m,z}| \sim 200{-}300$ Mev/c there is considerable deviation from the optical approximate formula (56), although the missing momenta at which the anomalous behavior (57) sets in are considerably greater than k_F, beyond the domain of applicability of the independent particle shell model used in the present paper.

The longitudinal momentum transfer in the incoherent rescattering of the struck proton in $A(e,e'p)$ reaction stems from the absence of an incoming proton plane wave in this case. Indeed, from the quantum-mechanical point of view the mere missing-momentum distribution (19) corresponds to interference of the amplitudes of the different positions at which the virtual photon strikes the proton. For each of these amplitudes the wave function of the spectator nucleons, after the struck proton leaves the target nucleus, will be distorted along the straight line that begins where the photon-proton interaction takes place. It is clear that the decomposition of the distortion of the spectator nucleon wave function into plane waves, besides the components with transverse momentum, contains components with longitudinal momentum. The asymptotic behavior (57) of the longitudinal momentum distribution is a consequence of the discontinuous distortion of the spectator nucleon wave functions. This discontinuity is connected with the θ-function appearing in the Glauber attenuation factor (8). It is evident that allowance for the finite longitudinal size, d_{int}, of the region where proton-nucleon interaction takes place must lead to smearing of the sharp

edge of the θ-function in Eq. (8). Evidently, d_{int} is approximately the proton radius. As a consequence of the smearing of θ-function in Eq. (8), the $p_{m,z}^{-2}$ law (57) will be replaced by a somewhat steeper decrease at high $|p_{m,z}|$. As a generalization of Eq. (8) to the case of finite d_{int} one can consider the substitutions

$$\theta(z) \Rightarrow \frac{\sqrt{\pi}}{d_{\text{int}}} \int_z^\infty d\xi \, \exp\left(-\frac{\xi^2}{d_{\text{int}}^2}\right), \qquad (58)$$

or

$$\theta(z) \Rightarrow \frac{1}{2}\left[1+\tanh\left(\frac{z}{d_{\text{int}}}\right)\right]. \qquad (59)$$

Of course, there is no serious theoretical motivation to use either of the prescriptions (58) or (59) at such $|p_{m,z}|$, where the missing-momentum distributions corresponding to the attenuation factor (8) and obtained with substitutions (58) or (59) start differing strongly. The latter can be used only to clarify the applicability limits of the standard Glauber model. Fortunately, it turns out that the kinematical range of the longitudinal missing momentum, where the Glauber model is still applicable, is quite broad. In Refs. 14 and 15 it was confirmed that the θ-function ansatz in the Glauber attenuation factor for the deuteron target works very well in the region $|p_{m,z}| \lesssim 500$ MeV/c. Our numerical calculations in the kinematical domain $|p_{m,z}| \lesssim 300$ MeV/c also show that introduction of the finite size of the interaction domain, $d_{\text{int}} \sim 1$ fm, leaves practically unchanged the standard Glauber-model predictions obtained with the θ-function in Eq. (8).

Notice, that due to the NN repulsive core, the probability of finding two nucleons at the same point in the target nucleus really is suppressed. This means that at high $|p_{m,z}|$, even without allowance for the finite d_{int} the tail of the longitudinal missing-momentum distribution will decrease considerably more abruptly when the short range NN correlation are taken into account. Since the NN correlation radius is ~ 1 fm, both the NN correlations and finite-d_{int} effects, as well as the effect of their interplay, can be neglected in the region $|p_{m,z}| \lesssim 300$ MeV/c under discussion.

However, when higher $p_{m,z}$ are concerned, this incompleteness of the Glauber model in the case of $A(e,e'p)$ scattering in the high-$|p_{m,z}|$ region makes questionable the mere possibility of using the measured missing-momentum distribution for deriving the information on the short-range NN correlations in nuclei: besides the genuine short-range NN correlations, the missing-momentum distribution at high $|p_{m,z}|$ probes the spatial extension of the nucleon as well. Note that this sensitivity of the high-$|p_{m,z}|$ tails to the nucleon size survives also at high Q^2, in the CT regime where off-diagonal inelastic rescattering makes a large contribution.

To conclude this section, we would like to emphasize that in the $A(e,e'p)$ reaction we face a situation which is quite different from small-angle hadron-nucleus scattering. In the latter case the incoming hadron plane wave exists. Hence θ-function effect in the Glauber attenuation factor (8) disappears and the Glauber-model predictions for the hadron-nucleus scattering are free of uncertainties connected with

the finite longitudinal size d_{int}. However, it is clear that this problem will arise again in quasielastic $(p,2p)$ scattering at large angle. The corresponding analysis of the reaction $(p,2p)$ in the kinematical range of the BNL experiment[34] will be presented elsewhere.

6. NUMERICAL RESULTS

In this section we present our numerical results from the Glauber model for the missing-momentum distribution and nuclear transparency in quasielastic $A(e,e'p)$ scattering. In order to avoid the complications with the target nucleus spin, we restrict ourselves to the case of the closed-shell nuclei ^{16}O and ^{40}Ca. We adjusted the oscillator shell model frequency ω_{osc} for these two nuclei to reproduce the experimental value of the root-mean-square radius of the charge distribution, $\langle r^2\rangle^{1/2}$. We used the values[35] $\langle r^2\rangle^{1/2}=2.73$ fm for ^{16}O, and $\langle r^2\rangle^{1/2}=3.47$ fm for ^{40}Ca, which correspond to the oscillator radius $r_{\mathrm{osc}}=(m_p\omega_{\mathrm{osc}})^{-1/2}$ equal to 1.74 fm for ^{16}O and 1.95 fm for ^{40}Ca. The difference between the charge distribution and the proton nuclear density connected with the proton charge radius was taken into account. This is a realistic model; we checked that it gives a charge density and SPMD in the region of $p_m\lesssim250$–300 MeV/c, which are practically indistinguishable from the results of more involved Hartree–Fock calculations.

As it was stated in Sec. 2, we use the exponential parametrization of the proton-nucleon elastic amplitude. The diffraction slope of the pN scattering was estimated from the relation

$$B_{pN}\approx\frac{\sigma_{\mathrm{tot}}^2(pN)(1+\alpha_{pN}^2)}{16\pi\sigma_{el}(pN)}.\tag{60}$$

In our calculations we define the pN cross sections and α_{pN} as mean values of these quantities for the pp and pn scattering. We borrowed the experimental data on pp, pn cross sections and α_{pp}, α_{pn} from the recent review.[36] In the region $Q^2\sim2$–10 GeV^2, the Q^2-dependence of the Glauber-model predictions for the missing-momentum distribution comes predominantly from the energy dependence of B_{pN} and $\sigma_{el}(pN)$. (We recall that the typical kinetic energy of the struck proton is $T_{\mathrm{kin}}\approx Q^2/2m_p$.) Typically B_{pN} rises from $B_{pN}\approx4.5$ GeV^{-2} at $Q^2=2$ GeV^2 to $B_{pN}\approx8$ GeV^{-2} at $Q^2=10$ GeV^2, and $\sigma_{el}(pN)$ falls from $\sigma_{el}(pN)\approx23$ mb at $Q^2=2$ GeV^2 to $\sigma_{el}(pN)\approx11.5$ mb at $Q^2=10$ GeV^2. In our kinematical domain, $\sigma_{\mathrm{tot}}(pN)$ slightly decreases with Q^2, $\sigma_{\mathrm{tot}}(pN)\approx43.5$ mb at $Q^2=2$ GeV^2 and $\sigma_{\mathrm{tot}}(pN)\approx40$ mb at $Q^2=10$ GeV^2. We recall that in the Glauber model the trajectories of the high-energy particles are assumed to be straight lines. For $Q^2\gtrsim2$ GeV^2, the struck proton has a momentum $\gtrsim2$ GeV/c, whereas the mean value of the momentum transfer in pN scattering is $cg\sim1/\sqrt{B_{pN}}\sim0.45$ GeV/c. Thus, there are reasons to believe that the Glauber formalism is still reliable at the lower bound of the kinematical domain of interest in the present paper, $Q^2\sim2$–10 GeV^2.

To illustrate the role of incoherent rescattering in inclusive $A(e,e'p)$ scattering, we present a systematic comparison of results obtained for the full Glauber theory with the $\Gamma^*\Gamma$ term in the FSI factor (26) included, and the truncated
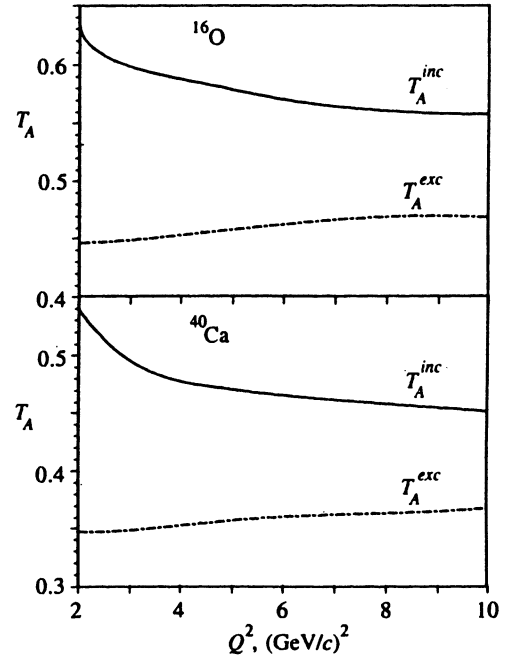

FIG. 1. The Q^2-dependence of nuclear transparency for ^{16}O$(e,e'p)$ and ^{40}Ca$(e,e'p)$ scattering. The solid curve is for the inclusive $(p_{m\perp},p_{m,z})$-integrated transparency T_A^{inc} as given by Eq. (39) and the dot-and-dash curve is for the exclusive transparency T_A^{exc} as given by Eq. (40).

version (the conventional DWIA) when $\Gamma^*\Gamma$ term is not included. We remind the reader that in the independent-particle shell model these two versions are relevant to the inclusive and exclusive conditions in $A(e,e'p)$ scattering, respectively.

The results for the integral nuclear transparencies T_A^{inc} and T_A^{exc} defined by Eqs. (39) and (40) are shown in Fig. 1. Because of the rise of $\sigma_{\mathrm{in}}(pN)$, T_A^{inc} slowly decreases in our kinematical range; T_A^{exc}, which is controlled by $\sigma_{\mathrm{tot}}(pN)$, is approximately flat. As one can see from Fig. 1, the replacement of $\sigma_{\mathrm{in}}(pN)$ by $\sigma_{\mathrm{tot}}(pN)$ considerably reduces the integral nuclear transparency and the difference between the T_A^{inc} and T_A^{exc} is much larger than the several percent correlation correction to T_A.[26] The computed values of T_A^{inc} and T_A^{exc} define the missing-momentum distribution $n_{\mathrm{eff}}(\mathbf{p}_m)$ $=w(\mathbf{p}_m)/T_A$ normalized to unity for the cases when the $\Gamma^*\Gamma$ term in the FSI factor is included (inclusive $A(e,e'p)$ scattering) and not included (exclusive $A(e,e'p)$ scattering), respectively.

When the acceptance domain D in the definition (3) includes all the missing momenta, the integral nuclear transparency depends only on the diagonal component of the proton one-body density matrix, i.e., the nuclear density. In contrast, the missing-momentum distribution and transparency $T_A(\mathbf{p}_m)$ as functions of $\mathbf{p}_m$ or $T_A(D)$ for a certain acceptance domain D as defined by Eq. (3) are controlled by the whole one-body density matrix. The results we report here are mostly for the realistic oscillator shell model one-body density matrix (18). In order to check the sensitivity of the results to the form of the one-body density matrix, we also report on calculations for the LDA parametrization (32)
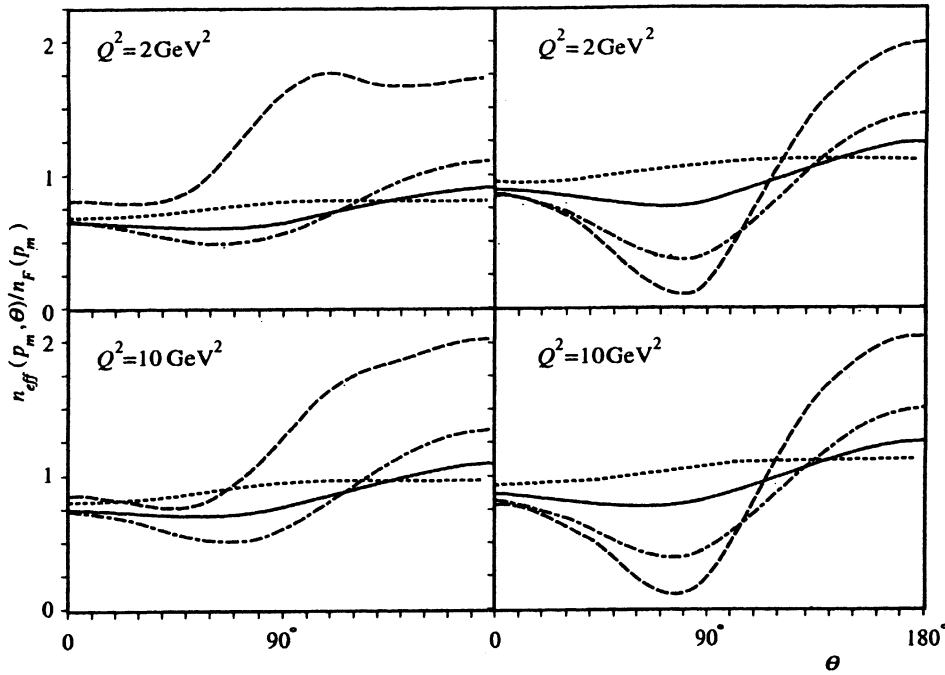
FIG. 2. Angular dependence of the inclusive missing-momentum distribution $n_{\rm eff}(p_m,\theta)$ in $^{16}{\rm O}(e,e'p)$ scattering calculated for FSI without (the left-hand boxes) and including (the right-hand boxes) the $\Gamma^*\Gamma$ terms as compared to the single-particle momentum distribution $n_F(p_m)$: the short-dashed, solid, dot-and-dash and long-dashed curves are for missing momentum $p_m = 150$, 200, 250, and 300 MeV/c, respectively.

of the one-body density matrix. A comparison of these two versions is very interesting for clarifying the accuracy and applicability limits of the LDA parametrization (32), which is widely used in the literature for nuclei with large nuclear mass number A.

In Figs. 2 and 3 we show the angular dependence of the ratio of the normalized missing-momentum distribution $n_{\rm eff}(p_m,\theta)$ to the SPMD $n_F(p_m)$ for $p_m = 150$, 200, 250 and 300 MeV/c at $Q^2 = 2$ and 10 GeV^2. The forward-backward asymmetry of this ratio is a consequence of the nonzero real part of the elastic pN amplitude. The appearance of a bump

for $p_m = 300$ MeV/c at $\theta \approx 100°$ for $Q^2 = 2$ GeV^2 in the full Glauber calculation with the $\Gamma^*\Gamma$ term is connected with the fact that momentum transfer in the incoherent rescattering is predominantly transverse. At $Q^2 = 10$ GeV^2, the bump evolves into a shoulder, which is related to the higher value of the diffraction slope. In contrast to the version with the $\Gamma^*\Gamma$ term, in the case without the $\Gamma^*\Gamma$ term we rather find a dip at $\theta \sim 80°$ for $p_m \sim 250$–300 MeV/c. This obviates a considerable distortion of the outgoing proton wave by the quantum FSI effects due to the elastic rescattering of the struck proton without the excitation of the residual nucleus.
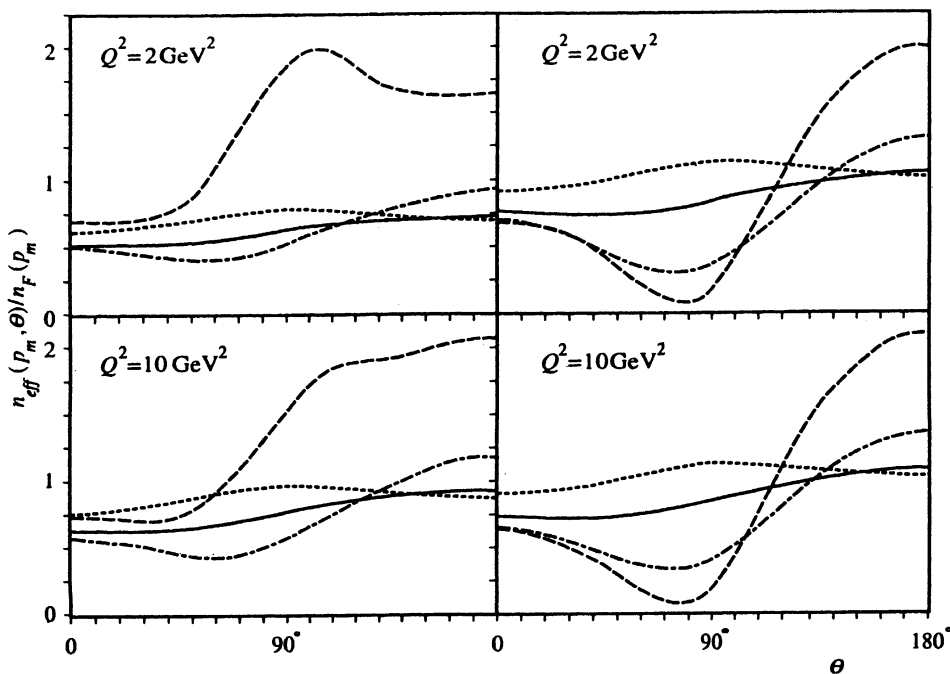
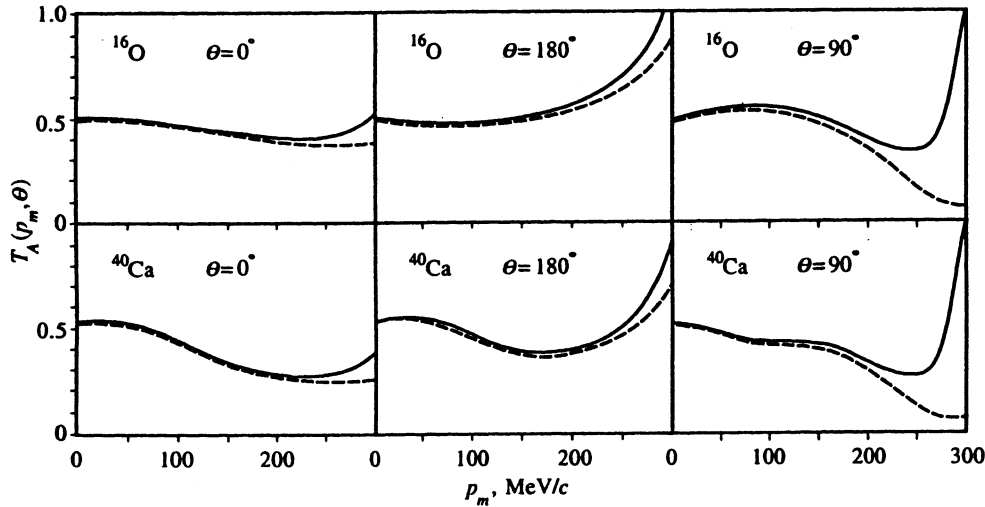FIG. 3. The same as in Fig. 2, but for $^{40}{\rm Ca}(e,e'p)$ scattering.

FIG. 4. The missing-momentum dependence of the nuclear transparency in parallel ($\theta=0,180°$) and transverse ($\theta=90°$) kinematics calculated (solid curve) for the full FSI including the $\Gamma^*\Gamma$ terms and (dashed curve) in the optical approximation not including the $\Gamma^*\Gamma$ terms.

Figure 4 illustrates the p_m-dependence of the nonintegrated nuclear transparency $T_A(p_m,\theta)$ for parallel ($\theta=0$), transverse ($\theta=90°$) and antiparallel ($\theta=180°$) at $Q^2=2$ GeV^2. Figure 4 demonstrates more clearly the relative role played in different kinematics by the absorption effects connected with the terms $\propto \Gamma(\Gamma^*)$ and incoherent rescattering effects related to the $\Gamma^*\Gamma$ term in the full FSI factor. We see that absorption generates a dip in the nuclear transparency in $A(e,e'p)$ reaction for exclusive conditions at $p_m\sim270-300$ MeV/c in the case of transverse kinematics ($\theta=90°$). With allowance for incoherent rescattering (when the $\Gamma^*\Gamma$ term is included), the nuclear transparency in transverse kinematics rises steeply at $p_m\gtrsim250$ Mev/c. Even in the (anti)parallel kinematics ($\theta=0$ and $\theta=180°$) the effect of $\Gamma^*\Gamma$ term becomes significant at $p_m\gtrsim250$ Mev/c. This effect is a mani-

festation of the longitudinal momentum transfer discussed in Sec. 5. The overall conclusion from Fig. 4 is that incoherent rescattering only becomes significant at a sufficiently large missing momenta, $p_m\gtrsim200-250$ MeV/c.

The corollary of the results shown in Fig. 4 is that the three-dimensional missing momentum distribution has a substantially nonfactorizable dependence on the transverse and longitudinal components of the missing momentum. In order to demonstrate the degree to which the $p_{m\perp}-p_{m,z}$ factorization is violated we present in Fig. 5 the nuclear transparency versus $p_{m\perp}$ at different $p_{m,z}$ for ^{40}Ca at $Q^2=2$ GeV^2. As one can see, the $p_{m\perp}-p_{m,z}$ factorization is manifestly violated. For the both versions, with and without the $\Gamma^*\Gamma$ term, transparency $T_A(\mathbf{p}_\perp,p_{m,z})$ is a lively function of $p_{m\perp}$, and $n_{eff}(\mathbf{p}_m)$ is strikingly different from the SPMD. This shows clearly, in

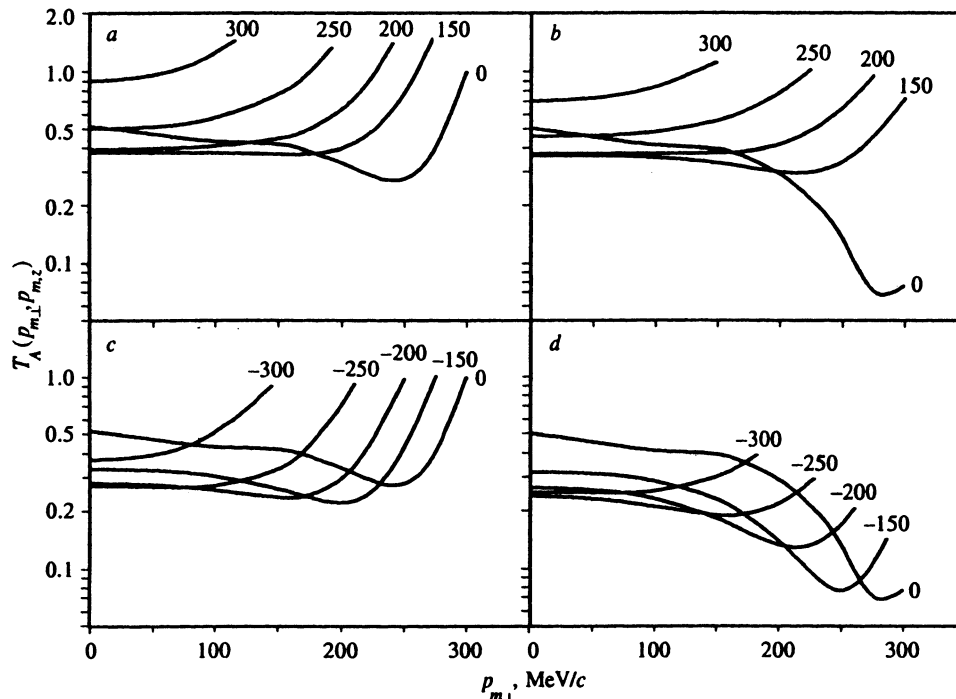FIG. 5. Nuclear transparency for ^{40}Ca$(e,e'p)$ scattering at $Q^2=2$ GeV^2 as a function of the transverse missing momentum $p_{m\perp}$ at different fixed values of the longitudinal missing momentum $p_{m,z}$ [MeV/c]. The boxes a and c are for the full FSI including the $\Gamma^*\Gamma$ terms, and the boxes b and d are for the optical approximation to FSI with the $\Gamma^*\Gamma$ terms not included.
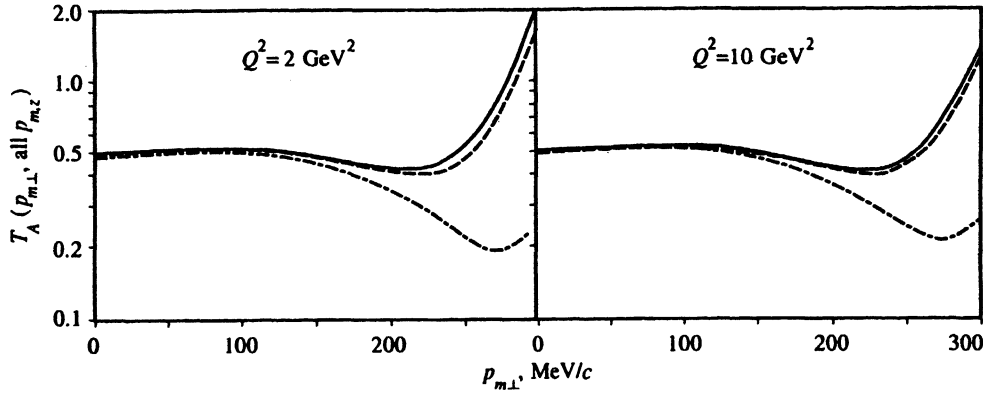
FIG. 6. Multiple-elastic rescattering decomposition of nuclear transparency in $^{16}O(e,e'p)$ scattering integrated over the longitudinal missing momentum. The dot-and-dash curve is for exclusive transparency ($\nu=0$), the solid curve shows inclusive transparency summed over all rescatterings (all ν), and the dashed curve shows the effect of including the first elastic rescattering ($\nu=0,1$).

particular, that the approach of Ref. 31 cannot be justified because the approximation (33) of Ref. 31 yields an almost $p_{m\perp}-p_{m,z}$ factorization form of $w(\mathbf{p}_m)$ with the same $p_{m\perp}$-dependence as for the SPMD.

In Figs. 6 and 7 we show nuclear transparency versus $p_{m\perp}$ for the full acceptance D versus the longitudinal momenta. The version with the $\Gamma^*\Gamma$ term corresponds to the full multiple incoherent scattering series (43) for $w_\perp(\mathbf{p}_{m\perp})$, whereas the case without the $\Gamma^*\Gamma$ term in the FSI factor is equivalent to keeping only the zeroth-order term in the series (43). Besides these two limiting cases, we present in Figs. 6 and 7 also the sum of the first two terms, $\nu=0$ and $\nu=1$, in the series (43). From Figs. 6 and 7 we conclude that in the kinematical domain the considered terms $\nu=0,1$ do practically saturate the inclusive $A(e,e'p)$ cross section. The incoherent rescatterings of the struck proton become important for $p_{m\perp}\gtrsim200$ MeV/c.

The $p_{m,z}$-dependence of nuclear transparency for the full acceptance in the transverse missing-momentum is shown in Fig. 8, the solid and dashed curves are for the versions with and without the $\Gamma^*\Gamma$ term. As the nuclear mass number increases, the clear-cut two-dip structure evolves for the case without the $\Gamma^*\Gamma$ term. Therefore, the attenuation for the FSI of the struck proton significantly distorts the missing-momentum distribution as compared to the PWIA case. Figure 8 shows that the $\Gamma^*\Gamma$ terms generate tails in the longitudinal missing-momentum distribution which already start taking over at $|p_{m,z}|\gtrsim200$ MeV/c. As in the case of a purely

parallel kinematics (see below), there is a considerable forward-backward asymmetry about $p_{m,z}=0$ connected with the nonzero α_{pN}. The integral forward-backward asymmetry A_{FB} defined as

$$A_{FB}=\frac{N(p_{m,z}>0)-N(p_{m,z}<0)}{N(p_{m,z}>0)+N(p_{m,z}<0)} \qquad (61)$$

[where $N(p_{m,z}>0)$ and $N(p_{m,z}<0)$ are the numbers of events with $p_{m,z}>0$ and $p_{m,z}<0$, respectively] is large, $A_{FB}\approx-(0.07-0.08)$, and approximately constant in our kinematical region ($Q^2\sim2-10$ GeV^2). The forward-backward asymmetry was suggested as a signature of the onset of CT[10–12] because at large Q^2 it is generated by inelastic (off-diagonal) scattering of the struck proton on spectator nucleons. The above cited forward-backward asymmetry for the nonzero α_{pN} obscures the use of this asymmetry as a CT effect, as a matter of fact, it exceeds by a factor of 2–4 the contribution to the asymmetry from the nondiagonal rescattering estimated in Refs. 11 and 12. Here we wish to notice that the nonzero α_{pN}, which is the origin of the forward-backward asymmetry in the Glauber model, is connected with the contributions to the elastic pN amplitude from the secondary reggeons. As is well known[37] the reggeon exchange requires a finite formation time that increases with hadron energy, for which reason the real part of the in-nuclear-medium elastic pN scattering amplitude, relevant to the $A(e,e'p)$ scattering, could partly differ from the in-
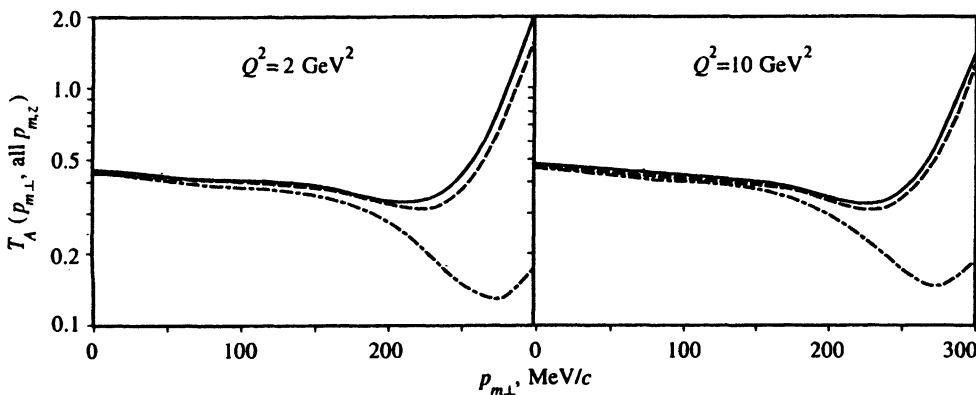

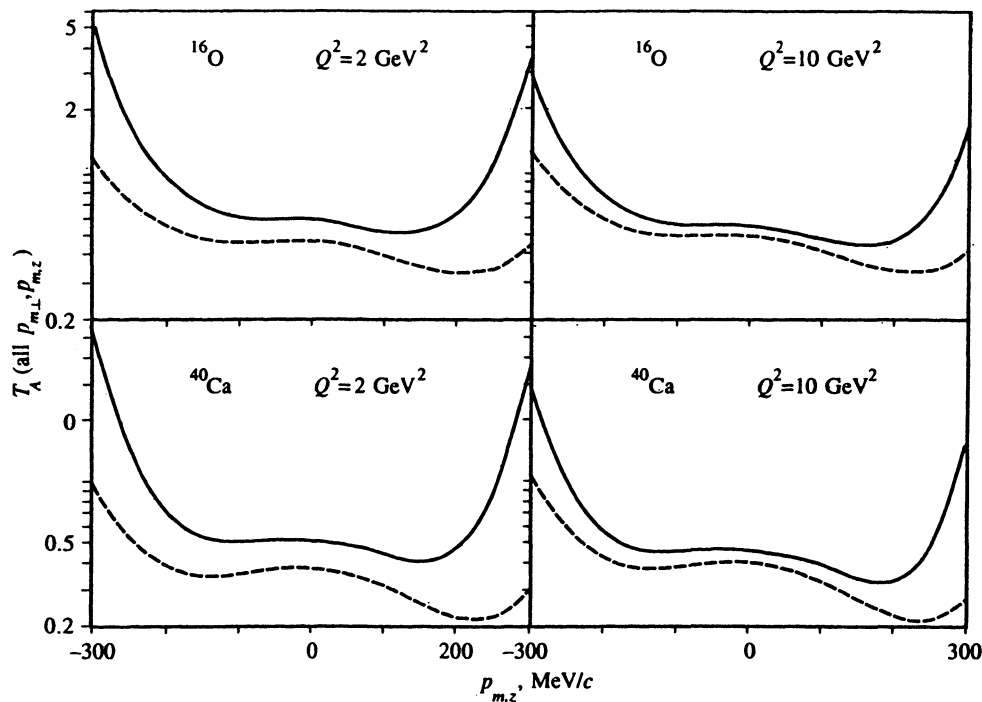FIG. 7. The same as in Fig. 6, but for $^{40}Ca(e,e'p)$ scattering.

FIG. 8. The longitudinal missing-momentum dependence of nuclear transparency integrated over the transverse missing momentum $p_{m\perp}$. The solid curves are for the full FSI including the $\Gamma^*\Gamma$ terms, the dashed curves are for the optical approximation to the FSI with the $\Gamma^*\Gamma$ terms not included.

vacuum pN scattering amplitude. In the absence of a rigorous theoretical model for the reggeon exchanges it will be difficult to disentangle the CT contribution to the forward-backward asymmetry. Nevertheless, any rise of A_{FB} with Q^2 will signal the onset of the CT effects, since the finite-formation-time effects for the reggeon exchange can only reduce the value of A_{FB} predicted in the standard Glauber model.

It is instructive to compare the $p_{m,z}$-dependence of nuclear transparency for parallel kinematics, $p_{m\perp}=0$, $\theta=0$, $180°$, shown in Fig. 4, and for the full acceptance in $\mathbf{p}_{m\perp}$, shown in Fig. 8. This comparison very clearly demonstrates that the major contribution from incoherent rescattering into large-$|p_{m,z}|$ tails comes from the region of the sufficiently large $p_{m\perp}$. The same conclusion can be drawn from the results presented in Fig. 5. We recall that just this pattern of the contribution to the missing-momentum distribution from the incoherent rescattering of the struck proton on the adjacent spectator nucleons at high-$|p_{m,z}|$ region was predicted in section 5 from the uncertainty relation. Thus, our numerical results give a clear-cut evidence of the need to treat the incoherent rescattering of the struck proton in $A(e,e'p)$ reactions in a quantum-mechanical manner.

The above discussion of the missing-momentum distribution can be summarized as follows: In the realistic model, distortions from incoherent rescattering ($\propto \Gamma^*\Gamma$ terms) take over at $p_m \gtrsim 200$ MeV/c, whereas distortions by coherent rescattering ($\propto \Gamma+\Gamma^*$ terms) dominate at smaller $p_m \lesssim 200$ MeV/c. However, even in this region of relatively small momenta the corrections for the incoherent rescattering are non-negligible. For instance, the integral nuclear transparencies T_A^{inc} and T_A^{exc} differ substantially, and the difference is due to the contribution of incoherent rescatterings in the inclusive $A(e,e'p)$. Because the contribution from the incoherent re-

scattering depends on the missing momentum, nuclear transparency measured in a restricted acceptance domain D may differ considerably from the integral nuclear transparency, even though in both cases the inclusive experimental conditions are imposed. Although the contribution from incoherent rescattering comes predominantly from high p_m, this does not imply automatically that nuclear transparency for sufficiently small p_m will be close to T_A^{exc}. As we have seen, even without the $\Gamma^*\Gamma$ term, the missing-momentum distribution will differ considerably from the PWIA case.

The above is especially important for experimentally disentangling CT effects in $A(e,e'p)$ scattering. Obviously, the definitive conclusions regarding CT can only be drawn if the experimental nuclear transparency is compared to the matching Glauber-model calculation for the same acceptance domain D. The sensitivity nuclear transparency to the acceptance domain D in the definition (3) is clearly demonstrated by the numerical results shown in Figs. 9 and 10. Here we present the results for the full Glauber model with the terms $\Gamma^*\Gamma$ (solid lines) for four different windows in the missing momentum. For the reference, we also show the inclusive and exclusive integral nuclear transparency computed using $\sigma_{in}(pN)$ (long-dashed lines) and $\sigma_{tot}(pN)$ (dot-and-dash lines). The results for the LDA one-body density matrix (32), shown in Figs. 9 and 10 by the dot-and-dash line, illustrate the sensitivity of the Glauber-model predictions to parametrizations of the one-body density matrix. We find quite a strong difference between predictions from the shell model and LDA parametrization, which varies with the missing-momentum window. As one can see from Figs. 9 and 10, for these acceptance windows the Glauber theory results with full shell model density matrix do differ considerably from both integral nuclear transparencies, T_A^{inc} and T_A^{exc}. An im-
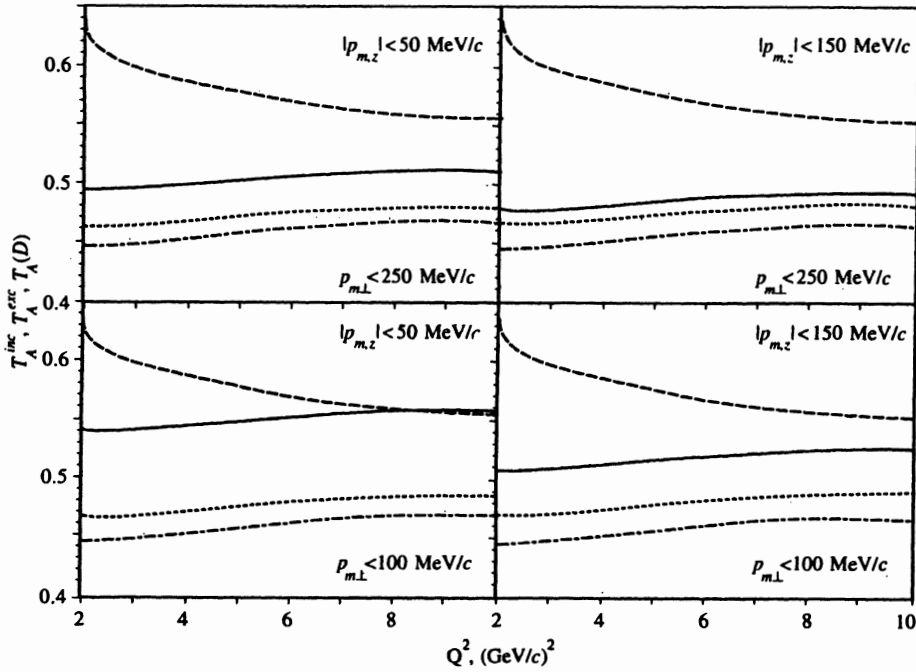
FIG. 9. The Q^2-dependence of nuclear transparency for $^{16}O(e,e'p)$ scattering at different windows D in the transverse $p_{m\perp}$ and longitudinal $p_{m,z}$ missing momentum compared with the inclusive transparency T_A^{inc} (the long-dashed curve) and the exclusive transparency (the dot-and-dash curve). The solid curve shows transparency $T_A(D)$ calculated with full treatment of FSI ($\Gamma^*\Gamma$ terms included) for the $(p_{m\perp}, p_{m,z})$-window D as shown in the corresponding box. The short-dashed curve is the same as the solid curve, but for the local density approximation for the one-body density matrix.

portant finding is that despite the increase of $\sigma_{in}(pN)$ in all kinematical domains considered, the nuclear transparency rises slightly with Q^2. We wish especially to emphasize the sensitivity of $T_A(D)$ to the missing-momentum window: the nuclear transparency varies by about ten percent even for moderate variations of the missing-momentum window. One would expect that intranuclear attenuation can neither be stronger than that given by σ_{tot} nor weaker than that given by σ_{in}, so naively

$$T_A^{inc} > T_A(D) > T_A^{tot}.$$

The results shown in Figs. 9 and 10 clearly demonstrate that the quantum-mechanical distortion effects do not amount to a simple attenuation. Namely, even at small p_m where incoherent elastic rescattering effects are still small, one can easily find the counterintuitive $T_A(D) > T_A^{inc}$.

The kinematical region $D = (p_{m\perp} < 250, |p_{m,z}| < 50$ MeV/ c) approximately corresponds to the kinematical conditions of the recent NE18 experiment.[8] In Fig. 11 we compare the experimental data[8] for ^{12}C and ^{56}Fe with the Glauber-model predictions. ^{12}C and ^{56}Fe are not closed-shell nuclei, $T_A(D)$
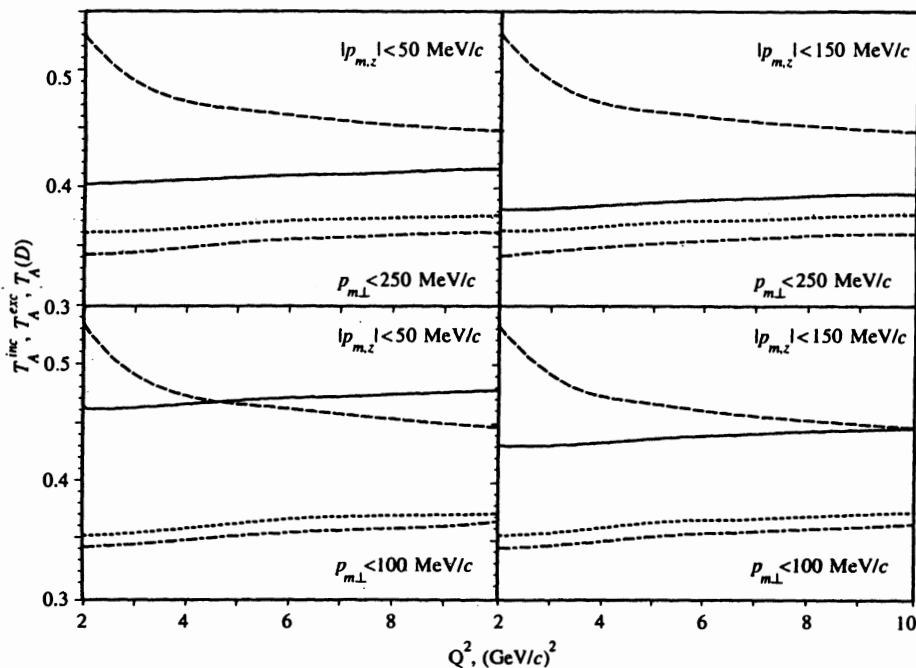

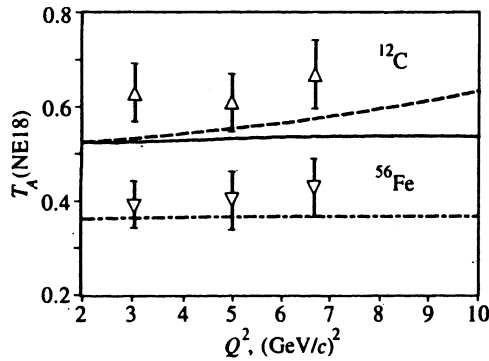FIG. 10. The same as in Fig. 9, but for $^{40}Ca(e,e'p)$ scattering.

FIG. 11. Predictions of nuclear transparency for a missing-momentum window $(p_{m\perp} < 250$ Mev/c, $|p_{m,z}| < 50$ Mev/c) in comparison with the NE18 determinations for ^{12}C (solid curve) and ^{56}Fe (dot-and-dash curve) nuclei. For the ^{12}C nucleus we also show the effect of color transparency (dashed curve) as evaluated in Ref. 17.

for these nuclei were calculated assuming that they interpolate between T_A^{exc} and T_A^{inc} as for the closed-shell ^{16}O and ^{40}Ca nuclei, respectively. We calculated T_A^{inc} and T_A^{exc} for ^{12}C using the parametrization of the nuclear density as a sum of Gaussians.[35] In the case of ^{56}Fe the three-parameter Gaussian model[35] was used. The difference between the charge-density distribution and the proton-density distribution was taken into account. The strong dependence of $T_A(D)$ on the missing-momentum window D (see Figs. 9 and 10) makes the full quantum-mechanical treatment of distortions imperative for a quantitative comparison between the theory and experiment. This full analysis of distortions has not been performed in the previous calculations of T_A, which were reviewed in great detail by Makins and Milner.[38] The only exception is Ref. 17, which discussed how $T_A(D_{NE18})$ interpolates between T_A^{exc} and T_A^{inc}, but the analysis of Ref. 17 only included the simplest distortions of the transverse momentum distribution from the incoherent rescattering. In Fig. 11 we also show the estimate[7] for CT effects.

Our values of $T_A(D_{NE18})$ are somewhat below the NE18 determinations. To this end, we recall that the NE18 analysis[8] uses certain model calculations of the denominator in Eq. (3). One of the key assumptions is that, modulo the overall normalization, the nuclear spectral function is identical to the PWIA spectral function. Our results show that this cannot be correct for the FSI effects, but the accuracy of the NE18 experiment is not sufficiently high to resolve the size of distortions found in our analysis. Furthermore, the NE18 analysis introduces renormalization of T_A by the factor 1.11 ± 0.03 for ^{12}C and 1.22 ± 0.06 for ^{56}Fe nuclei, which renormalization is meant to account for the missing strength associated with the large-p_m component of the spectral function coming from short-range NN correlations. Similar correction for the missing strength must be included, both in the numerator and denominator of Eq. (3), in our analysis too. One must bear in mind, though, that the SRC and FSI effects cannot easily be separated. For instance, the recent work[14] on the ^{4}He$(e,e'p)$ reaction found a strong interference between the FSI and short-range correlation effects, which is stronger than the SRC effect and which makes the corrections for the

NN correlations to the numerator and denominator different. For this reason, those renormalization effects must be regarded as an indication of the accuracy of the shell-model calculations of $T_A(D_{NE18})$. More sophisticated calculations which include NN correlations and correct treatment of FSI simultaneously are required for the theory to confront the higher accuracy experimental data on T_A.

The difference between the predictions from the full-shell model and the LDA one-body density matrices shown in Figs. 9 and 10 illustrates a substantial sensitivity of FSI distortions of the three-dimensional missing-momentum distribution to the off-diagonal elements of one-body density matrix. To gain more insight into the sensitivity to the one-body density matrix, in Fig. 12 we compare the results for the $p_{m,z}$-integrated nuclear transparency as a function of $p_\perp$ for the full-shell model and LDA one-body density matrices (the solid and long-dashed curves, respectively) at $Q^2 = 2$ GeV^2. The difference is very large at small $p_{m\perp}$, reaching $\sim 20\%$ for ^{40}Ca nucleus, the full-shell model also predicts much a deeper minimum in the transparency at $p_{m\perp} \sim 225$ MeV/c, beyond the crossover at $p_{m\perp} \sim 150$ MeV/c. The difference between the full-shell model and LDA results becomes even more striking if one compares the nonintegrated nuclear transparencies. In Figs. 13 and 14 we present such a comparison for the transverse kinematics. The results for the parallel kinematics are presented in Figs. 15 and 16. As one can see from Figs. 13–16, the LDA (32) underestimates nuclear transparency at small p_m and overestimates in the high-p_m region. For $p_m \sim 0$, predictions from the full-shell model and LDA density matrices differ by $\gtrsim 20\%$.

One might have expected the LDA (32) to become more reliable with increasing A; this expectation is not born out by our calculations, the difference between the full-shell model and LDA predictions does not reveal any tendency to disappear with increasing nucleus mass number. This is one more reminder that quantum interference effects play an important role in the FSI of the struck proton in the nuclear medium. The qualitative failure of the LDA even for the heavy ^{40}Ca nucleus can be explained by the large contribution to the cross section for $A(e,e'p)$ scattering from the events corresponding to the proton ejecting from the nucleus surface. Evidently there are no good reasons to expect LDA to be reliable in the surface region.

7. CONCLUSIONS

The purpose of this work has been to develop the Glauber-theory description of the missing-momentum distribution in quasielastic $A(e,e'p)$ scattering in the region of moderate missing momenta, $p_m \lesssim 300$ MeV/c. Such a description is applicable at high energy, $Q^2 \sim 2$–10 GeV^2. We have found a novel effect of interaction between two trajectories which enter the calculation of the FSI-modified one-body density matrix and originates in the incoherent elastic rescattering of the struck proton, and have presented for the first time a consistent treatment of this effect in a realistic model.

Our numerical results show that the missing-momentum distribution in $A(e,e'p)$ scattering is substantially affected by FSI effects compared to the PWIA case for both the in-
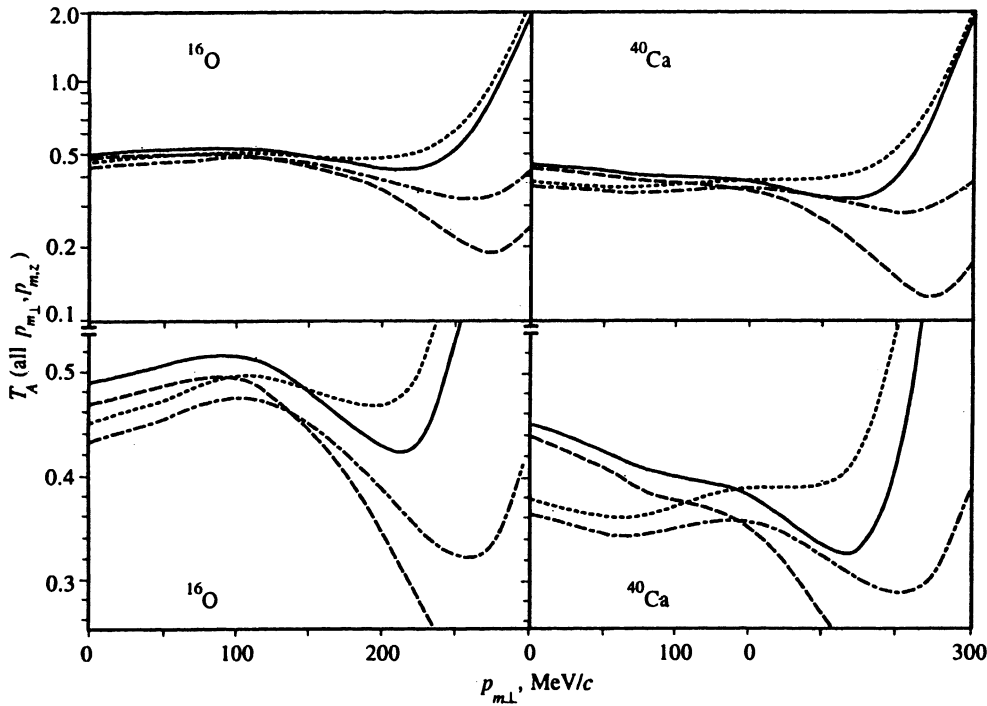
FIG. 12. The transverse missing-momentum dependence of the nuclear transparency integrated over the longitudinal missing momentum $p_{m,z}$ for the full-shell model calculation with the $\Gamma^*\Gamma$ terms included (solid curve) and not included (long-dashed curve), and for the local-density approximation with the $\Gamma^*\Gamma$ terms included (short-dashed curve) and not included (dot-dashed curve). $Q^2=2$ GeV^2. The bottom boxes show the same curves on a blown-up scale.

clusive and exclusive conditions. At large Q^2 the difference between the integrated nuclear transparencies T_A^{inc} (the $\propto \Gamma^*\Gamma$ terms included) and T_A^{exc} (only the $\propto \Gamma^*+\Gamma$ terms included) becomes relatively weak, and small values of T_A are mostly due to attenuation from the $\propto \Gamma^*+\Gamma$ terms. In the missing-momentum distribution, the distortion effects from the incoherent rescattering ($\propto \Gamma^*\Gamma$ terms) takes over for $p_m \gtrsim 200$ MeV/c. The distortion effects connected with coherent rescatterings ($\propto \Gamma+\Gamma^*$ terms) of the struck proton dominate at $p_m \lesssim 200$ MeV/c, but even in this region the corrections due to incoherent rescattering are not negligible. Our important finding is that, apart from the transverse missing-momentum distribution, incoherent rescattering also substantially affects the longitudinal momentum distributions

at high missing momentum. This distortion of the longitudinal momentum distribution is of a purely quantum-mechanical origin.

Our calculations show that the forward-backward asymmetry connected with the elastic (diagonal) rescattering of the struck proton on the spectator nucleons is larger than expected from the CT effects by the factor about 2–4 for $Q^2 \sim 5$–10 GeV^2. In the region $Q^2 \sim 2$–3 GeV^2 the expected role of the CT effects is negligible. This casts a doubt on the use for the forward-backward asymmetry as a clean signal of the onset of CT in the CEBAF kinematical region.

Using the calculated three-dimensional missing-momentum distribution, we studied the energy dependence of the nuclear transparency for a few kinematical domains. Our results show that despite the rise of $\sigma_{\text{in}}(pN)$, reducing the integral nuclear transparency, the nuclear transparency for the kinematical domains with $p_m \lesssim 250$ MeV/c even slightly increases with Q^2. We have compared for the first
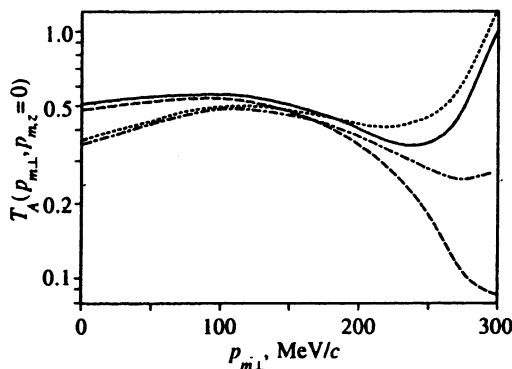

FIG. 13. Nuclear transparency in $^{16}\text{O}(e,e'p)$ scattering in transverse kinematics $p_{m,z}=0$ for the full-shell model calculation with the $\Gamma^*\Gamma$ terms included (solid curve) and not included (long-dashed curve), and for the local-density approximation with the $\Gamma^*\Gamma$ terms included (short-dashed curve) and not included (dot-dashed curve); $Q^2=2$ GeV.
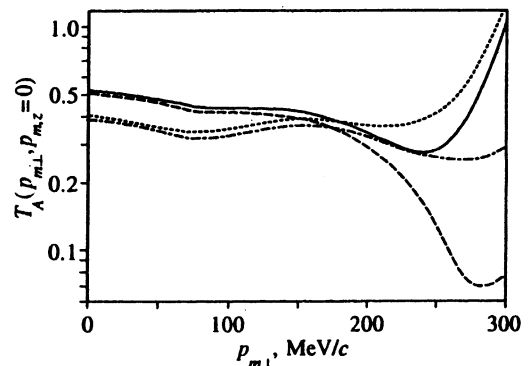

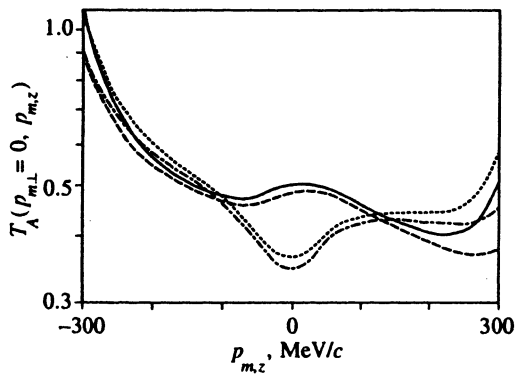FIG. 14. The same as Fig. 13, but for $^{40}\text{Ca}(e,e'p)$ scattering.

FIG. 15. Nuclear transparency in $^{16}O(e,e'p)$ scattering in parallel kinematics $p_{m\perp}=0$ for the full-shell model calculation with the $\Gamma^*\Gamma$ terms included (solid curve) and not included (long-dashed curve), and for the local-density approximation with the $\Gamma^*\Gamma$ terms included (short-dashed curve) and not included (dot-and-dash curve); $Q^2=2$ GeV^2.

time the Glauber-model prediction with the recent data from NE18 experiment[8] accurately taking into account the kinematical restrictions in the missing momentum. The energy dependence obtained in the present paper is close to that observed in Ref. 8. Our detailed calculations of distortion effects also highlight the limited applicability of treatments of FSI effects based on the conventional DWIA and local-density approximations.

Our important observation is that in the case of $A(e,e'p)$ reaction the Glauber formalism is incomplete at sufficiently high longitudinal missing momenta. We have shown that the standard Glauber-model ansatz for the attenuation factor causes an anomalously slow decrease $(\propto|P_{m,z}|^{-2})$ of the missing-momentum distribution at high longitudinal missing momenta. Such a tail is an artifact of neglecting the finite longitudinal size of the region where the struck proton interacts with the spectator nucleon. Allowance for the finite interaction size must drastically change the Glauber-model predictions at $|p_{m,z}| \gtrsim 500$ MeV/c. We checked that corrections to the predictions of the standard Glauber approach are still negligible at $|p_{m,z}| \lesssim 300$ MeV/c. It is important that the same incompleteness is inherent and persistent also in the color transparency regime at high Q^2,
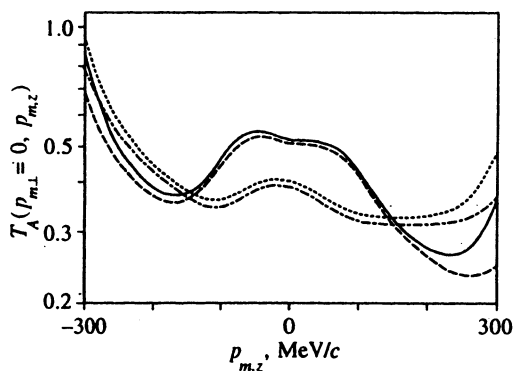
where the Glauber theory must be complemented by the off-diagonal transitions.

The sensitivity of the FSI effects to the finite longitudinal size of the interaction zone for pN collision has important implications for the interpretation of the experimental data on $A(e,e'p)$ scattering in terms of the short-range NN correlations in nuclei. Specifically, it makes clear that besides the short-range NN correlation the measured missing-momentum distribution becomes sensitive at high missing momenta to the spatial extension of the nucleon as well. The results of the detailed analysis of the influence of finite nucleon size on the missing-momentum distribution at high missing momenta will be presented elsewhere.

[1] A. H. Mueller, in Proceedings of the XVII Rencontre de Moriond, Les Arcs, France. Ed. by Tranh Thanh Van, Editions Frontieres, Gif-sur-Yvette (1982), p. 13.
[2] S. J. Brodsky, in Proceedings of the XIII International Symposium on Multiparticle Dynamics, Volendam, Netherlands, Ed. by E. W. Kittel, W. Metzger, and A. Stergion, World Scientific, Singapore (1982), p. 963.
[3] A. B. Zamolodchikov, B. Z. Kopeliovich, and L. I. Lapidus, JETP Lett. 33, 595 (1981).
[4] G. Bertsch, S. J. Brodsky, A. S. Goldhaber, and J. R. Gunion, Phys. Rev. Lett. 47, 267 (1981).
[5] B. Z. Kopeliovich and B. G. Zakharov, Sov. J. Nucl. Phys. 46, 911 (1987).
[6] J. Nemchik, N. N. Nikolaev, and B. G. Zakharov, in Proceedings of the Workshop on CEBAF at Higher Energies. Ed. by Nathan Isgur and Paul Stoler, CEBAF (1994), p. 415.
[7] N. N. Nikolaev, A. Szczurek, J. Speth et al., Nucl. Phys. A 567, 781 (1994).
[8] NE18 Collaboration: N. C. R. Makins, R. Ent, M. S. Chapman et al., Phys. Rev. Lett. 72, 1986 (1994); T. G. O'Neill, W. Loremzon, P. Anthony et al., Phys. Lett. B 351, 93 (1995).
[9] R. J. Glauber, in Lectures in Theoretical Physics, Vol. 1, ed. by W. Brittain and L. G. Dunham. Interscience Publ., New York (1959); R. J. Glauber and G. Matthiae, Nucl. Phys. B 21, 135 (1970).
[10] B. K. Jennings and B. Z. Kopeliovich, Phys. Rev. Lett. 70, 3384 (1993).
[11] N. N. Nikolaev, A. Szczurek, J. Speth et al., Phys. Lett. B 317, 287 (1993).
[12] A. Bianconi, S. Boffi, and D. E. Kharzeev, Phys. Lett. B 325, 294 (1994).
[13] S. Boffi, C. Giusti, and F. D. Pacati, Phys. Rep. 226, 1 (1993).
[14] A. Bianconi, S. Jeschonnek, N. N. Nikolaev, and B. G. Zakharov, Phys. Lett. B 338, 123 (1994).
[15] A. Bianconi, S. Jeschonnek, N. N. Nikolaev, and B. G. Zakharov, Phys. Lett. B 343, 13 (1995).
[16] N. N. Nikolaev, A. Szczurek, J. Speth et al., Nucl. Phys. A 582, 665 (1995).
[17] N. N. Nikolaev, A. Szczurek, J. Speth et al., Phys. Rev. C 50, R1296 (1994).
[18] A. Bianconi, S. Jeschonnek, N. N. Nikolaev, and B. G. Zakharov, Preprint KFA-IKP(Th)-14-1995, Jülich, (1993).
[19] T. de Forest Jr., Nucl. Phys. A 392, 232 (1983).
[20] B. Z. Kopeliovich and B. G. Zakharov, Phys. Rev. D 44, 3466 (1991).
[21] B. Z. Kopeliovich and B. G. Zakharov, Phys. Lett. B 264, 434 (1991).
[22] O. Benhar, S. Fantoni, N. N. Nikolaev, and B. G. Zakharov, Phys. Rev. Lett. 74, 3565 (1995).
[23] J. W. Van Orden, W. Truex, and M. K. Banerjee, Phys. Rev. C 21, 2628 (1980); S. Fantoni and V. R. Pandharipande, Nucl. Phys. A 427, 473 (1984); S. C. Pieper, R. B. Wiringa, and V. R. Pandharipande, Phys. Rev. C 46, 1741 (1992).
[24] K. Gottfried, Ann. Phys. 21, 29 (1963); W. Czyz and K. Gottfried, Nucl. Phys. 21, 676 (1961); Ann. Phys. 21, 47 (1963).

FIG. 16. The same as in Fig. 15, but for $^{40}Ca(e,e'p)$ scattering.

[25] N. Srivastava, Phys. Rev. B **135**, 612 (1964); D. U. L. Yu, Ann. Phys. (NY) **38**, 392 (1966).

[26] N. N. Nikolaev, A. Szczurek, J. Speth *et al.*, Phys. Lett. B **317**, 281 (1993).

[27] G. D. Alkhazov, S. I. Belostotsky, and A. A. Vorobyev, Phys. Rep. C **42**, 89 (1978).

[28] L. L. Frankfurt, M. I. Strikman, and M. B. Zhalov, Nucl. Phys. A **515**, 599 (1990).

[29] T.-S. H. Lee and G. A. Miller, Phys. Rev. C **45**, 1863 (1992).

[30] A. Kohama, K. Yazaki, and R. Seki, Nucl. Phys. A **551**, 687 (1993).

[31] A. S. Rinat and B. K. Jennings, Nucl. Phys. A **568**, 873 (1994).

[32] J. Negele and D. Vautherin, Phys. Rev. C **5**, 1472 (1971); C **11**, 1031 (1974).

[33] A. Kohama, K. Yazaki, and R. Seki, Nucl. Phys. A **536**, 716 (1992).

[34] A. S. Carroll, D. S. Barton, G. Bunce *et al.*, Phys. Rev. Lett. **61**, 1698 (1988).

[35] H. de Vries, C. W. de Jager, and C. de Vries, Atomic Data and Nuclear Data Tables **36**, 496 (1987).

[36] C. Lechanoine-LeLuc and F. Lehar, Rev. Mod. Phys. **65**, 47 (1993).

[37] B. Z. Kopeliovich, L. I. Lapidus, and A. B. Zamolodchikov, Sov. J. Nucl. Phys. **35**, 75 (1982).

[38] N. C. R. Makins and R. G. Milner, Preprint MIT-LNS 94-79, Cambridge (1994).